



**FAST SCINTILLATORS
FOR HIGH RADIATION LEVELS**

**Stan Majewski and Carl Zorn
Continuous Electron Beam Accelerator Facility
12,000 Jefferson Avenue
Newport News, Virginia, U.S.A. 23606**

**Contribution to Instrumentation in High Energy Physics, edited by
Fabio Sauli, and to be published by World Scientific Publishing Co. Pte.
Ltd. in 1992.**

FAST SCINTILLATORS FOR HIGH RADIATION LEVELS

Stan Majewski and Carl Zorn
CEBAF, Physics Division
12,000 Jefferson Avenue
Newport News, Virginia, U.S.A. 23606
Email: MAJEWSKI and ZORN@CEBAF

Part I

Crystal Scintillators

Stan Majewski

Part II

Plastic and Liquid Organic Scintillators

Carl Zorn

ABSTRACT

The development of new high luminosity hadron colliders (SSC and LHC) has posed a number of new challenges to traditional detector technologies. In addition to the expected problems of cost, project management, fast timing, energy resolution, occupancy levels, etc., some detectors (particularly calorimeters) face new problems due to the unusually high radiation levels expected in the forward regions of the beam-beam intersections. Although not alone in this category, scintillators face this last problem as probably the determining factor for their use in the high radiation areas, especially in the calorimetric detectors.

This article is a review of ongoing developmental work to make scintillators a viable and important element of the next generation of high energy physics detector systems. Although the key problem is that of radiation tolerance, attention has to be paid to such questions as fast timing capability, energy resolution, light output, and photodetector spectral sensitivity and quantum efficiency in order to produce a realistic solution.

It is the intent of the authors to show that although the final solutions may not exist at present, the achievements of the past few years show that the solution is probably realizable with proper effort and attention within the time scale envisioned for the construction of the new colliders.

Contribution to Instrumentation in High Energy Physics, edited by Fabio Sauli, and to be published by World Scientific Publishing Co. Pte. Ltd. in 1992.

**FAST SCINTILLATORS
FOR HIGH RADIATION LEVELS**

**Part I
Crystal Scintillators**

Part I: Crystal Scintillators

I.1. Introduction

With the increasing energies and interaction rates of the upgraded detectors either planned or under construction for the presently operational accelerators, and the detectors intended for experiments at the future machines such as SSC, LHC, UNK, K-factories and RHIC (in p-p experiments), there is an ever increasing demand for fast and radiation hard dense scintillators or Cherenkov radiators for high resolution electromagnetic calorimeters. The expected interaction rate will be around $10^8/\text{sec}$ at the SSC and up to $2.5 \times 10^9/\text{sec}$ at the high luminosity version of the LHC. The differences in calculated radiation dose rates of two orders of magnitude exist between RHIC and SSC, with LHC at the top of the list ^{1, 2}. But even in the RHIC case, even if a small fraction of the beam is accidentally dumped or scattered into a detector, the damage can be serious. Figure I.1.1 shows the comparison of the calculated fluxes of secondary particles and integrated radiation doses per year for the SSC ($L = 1 \times 10^{33} \text{ cm}^{-2}\text{s}^{-1}$) and the high luminosity version of the LHC ($L = 4 \times 10^{34} \text{ cm}^{-2}\text{s}^{-1}$) ³. The intensity scale factor between these two machines is 27^1 .

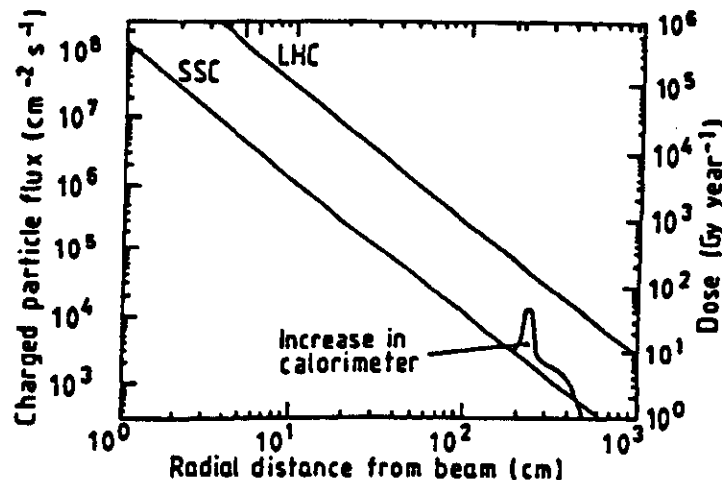


Figure I.1.1: The expected charged particle flux as a function of the radial distance from the interaction point for the SSC and the LHC with the corresponding integrated radiation doses/year due to ionization energy deposit ³. The energy deposit will locally increase in calorimeters due to the showering process.

Heavy scintillating materials make possible the construction of hermetic detectors without local defects. The main advantage of fully active crystal scintillator electromagnetic calorimeters is their excellent energy resolution, making them the best tools for electron and gamma detection. This was found to be necessary for efficient electron identification at the SSC ⁴. The most stringent limit on resolution is set by the requirement to study the 2g decay mode of a light Higgs ⁵. In several recent review articles ^{3, 6, 7, 8} the analysis of possible solutions was performed. First, it was concluded that no candidates for high resolution calorimetry were available presently for the most forward regions due to

respectively. Many crystal scintillators have several scintillation components which are usually divided into "fast" and "slow" ones. The basic mode of operation is to use the fast component and to try to desensitize readout to the slow components. A classical example of this technique is barium fluoride, where much effort went into designing photocathodes insensitive to the slow (~600 ns) decay component (see section I.2). The effects of radiation damage in crystal and glass scintillators are primarily due to damage to transmission properties of materials, while damage to intrinsic scintillation yield has not been observed in some cases even up to the doses of 1 GRad (10 MGray).

To illustrate the serious problems encountered one might take a look at cerium. Cerium is an excellent rare-earth scintillator and can be incorporated into a wide range of matrices, but the speed of its emission is only marginally acceptable. The scintillation emission is due to the characteristic fast allowed 5d-4f dipole transition in Ce^{3+} in the region of 300 to 500 nm, depending on the host matrix. Only lattices in which Ce^{3+} ions fit and the formation of Ce^{4+} quenching centers is minimized are suitable for this class of scintillators⁹. Especially interesting are high density matrices. Examples of cerium scintillators are: cerium-doped gadolinium silicate (Gd_2SiO_5), yttrium aluminate ($YAlO_3$), rhenium aluminate ($ReAlO_3$), barium fluoride (BaF_2), and cerium fluoride (CeF_3).

It seems that at the time of writing this review there is one material which satisfies most of the above listed and discussed criteria: barium fluoride. Recently it was preselected as a possible solution for the GEM SSC detector. The planned detector will have a total of about 16,000 crystals. In section I.2 we will discuss properties and applications of this very important crystal scintillator. But even barium fluoride will not survive the radiation doses expected in the very forward regions of the SSC and LHC. A fast detector with liquid scintillator capillaries replacing scintillating fibers is a possible candidate for that region. Other possible candidates except BaF_2 are: CeF_3 , cerium doped gadolinium orthosilicate ($Gd_2SiO_5:Ce$), pure CsI, and lead fluoride (PbF_2), a Cherenkov radiator material, listed in the order of their overall judged applicability.

Depending on the count rate and magnetic field expected in a particular region of a detector, different readout methods are applicable to crystal scintillators. In general, these can be silicon photodiodes, vacuum photodiodes, phototriodes and phototetrodes, and finally higher gain devices such as new type mesh photomultipliers to be used in magnetic fields and at high rates. It was shown, for instance, that the Hamamatsu photomultiplier type 2490 with 16 transmission dynode stages works even at a magnetic field of 1.5 Tesla, and at tilting angles up to 50° still can provide a gain of more than 10^3 ¹³. New hybrid photomultipliers with a silicon PIN or APD active "amplifying" element are under development¹⁴⁻¹⁸. Efforts are also under way to minimize the effect of Cherenkov light produced in the photomultiplier as a result of the passage of particles through the PMT window by working on a special design of a thin glass photocathode support¹⁹. An example of a large readout system is the CLEO CsI(Tl) electromagnetic calorimeter where crystals are read by silicon photodiodes. This system is too slow for most of the future applications (shaping time of several microseconds), but new versions are being prepared with pure CsI in mind and shaping time in the range of 100 ns (see section I.5).

Table I - cont.
List of candidates for fast and radiation hard crystal scintillators

MATERIAL	DECAY Fast Comp. (ns)	FAST EMISSION @ λ (nm)	FAST LIGHT YIELD (BIALKALI PM) %, NaI(Tl) = 100 (<i>pe/MeV</i>) (<i>phot./MeV</i>)	RADIA TION LIMIT (Rad)	DECAY Slow Comp (ns).	DENSITY (g/cm^3)	RAD. LENGTH (cm)	MOLIERE RADIUS	NUCL. INT. LEN. (cm)	dE/dX (MeV /cm)	HYGRO- SCOPIC (?)	REFR. INDEX @Peak	$\Delta L/\Delta T$ @20 C (%/C)
LiYbF ₄	≤25	400-500	(-BaF ₂)	high?		6.09	1.56	2.70					
BaLiF ₃	<1 (UV), <25 (vis.)	228,252, 435-440	(-BaF ₂ in UV)			5.24	2.13	3.13					
LiBaF ₃	1.9	203,234	-3,(900 - -BaF ₂)			4.9	2.3						
KYF ₄ :Rb	1.9	140-190	(-BaF ₂)			3.6							
K ₂ YF ₅			(-BaF ₂ @ 80°K)			-2							
RbF	1.3	203, 234, 380	(→ -BaF ₂)		<i>No slow component</i>	3.6					yes		
CaCl	.88	240, 270	(900--BaF ₂ @ 80°K)		>500 @390nm	4.0					no		
CaBr	0.07 (!)	250	(20)		>500 @390 nm	4.4					no		
CaBr	1.34±0.05 @80°K	250	(-BaF ₂ @ 80°K)			4.4					no		
RbCaF ₃	=1		(-BaF ₂)			2.83							
KCaCl ₃	=1@ 80°K		(-BaF ₂ @ 80°K)										
KCaF ₃	<2	140-190	(-BaF ₂)			3.0							
CsCaCl ₃	<1	250, 305	(est. 5000)			2.9							
CsSrCl ₃	=1		(-BaF ₂)										
LSO:Ce	-40	420	75			7.4	1.14						
CdI ₂	3	540	10	-10*7		5.67	1.5	3					
Y ₃ Al ₅ O ₁₂ : Ce (0.4 mol%)	65	550	(14000)			4.56	3.5	3.2					
BaCl ₂	1.2, 3.5		(25000)		58, -μs?	3.9							
CeCl ₃	4.4, 23		(28500)		70, -μs?	3.9							
BaI ₂	6	190-340			2500 @450nm	5.15					no, but air unstable		

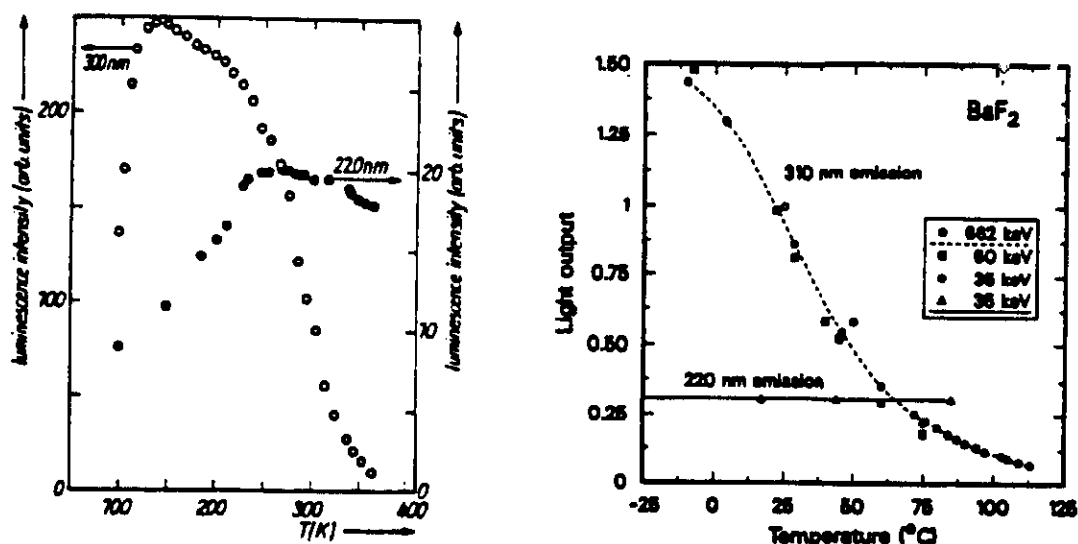


Figure I.2.2: Temperature dependence of the fast and slow emissions of barium fluoride ²⁸ (left) and ³⁰ (right).

Its fast subnanosecond decay component makes barium fluoride operable at high rates, and it was shown to be one of the most radiation hard scintillators, despite the fact that the effects of radiation damage on the performance of long modules were still not evaluated to satisfaction. Another big advantage of barium fluoride is that the intensity of the fast component is independent of temperature, while the intensity of the slow component decreases with increasing temperature ²⁶⁻³⁰ as shown in figures I.2.1 and I.2.2. This property of BaF₂ was actually exploited in order to yield a better gamma-ray energy resolution by cooling a BaF₂ crystal to 243 °K ³¹.

For applications in the precision crystal calorimetry, however, barium fluoride has at least two drawbacks: (1) a rather long radiation length and large Moliere radius, and (2) a small ratio of hadronic absorption length to radiation length making e/hadron separation difficult. Other disadvantages of BaF₂ include its mechanical fragility (it cleaves easily), and difficulty in detecting the short UV light component. It is also rather expensive. This is further compounded by a slight hygroscopic nature of BaF₂ which was found to affect the light yield ³²⁻³⁴. After repolishing, the crystals regain their transmission and light yield. Taking all this into consideration, a vigorous research was initiated, especially in Europe, to identify a possible replacement for BaF₂, such as CeF₃ or other new materials ⁸. But as of today, barium fluoride is a unique high density (4.88 g/cm³) scintillator with subnanosecond timing properties (110-160 ps FWHM) ³⁵⁻³⁹ with three emission spectra with peaks at 195 and 220 (fast component) and 310 nm (slow component) ^{28, 40, 41}. The fast components have fast decay time constants measured to be 0.6-0.79 ns ³⁵ and 0.85-0.88ns ⁴⁰⁻⁴³ (figure I.2.3) and the slow component was measured in the range of 100-1000 ns.

The fast emission in BaF₂ was explained to be due to a so-called "radiative core-valence transition" or "cross-over transition" following the direct electron-hole recombination ^{40, 43-46}. The same phenomenon also occurs in CsF. A different mechanism of self-trapped

components were identified with decay times of 730 ± 60 ns (80%) and 240 ± 30 ns (20%)⁴⁷. The weighted average is 630 ns which is in good agreement with previous results. In a recent high statistics measurement two slow components of BaF₂ emission were identified with 340 ns and 920 ns decay constants³⁰ (figure I.2.5).

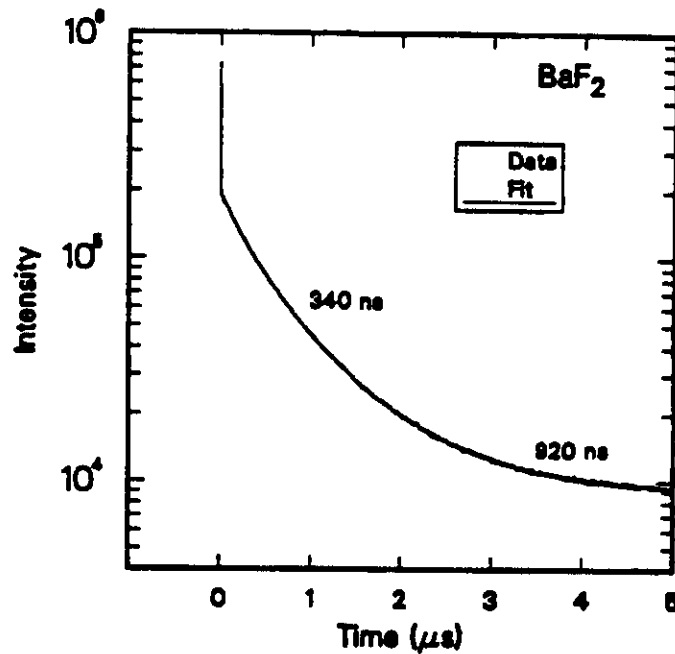


Figure I.2.5: Single-photon measurement of the scintillation decay of BaF₂ showing the fast and two slow components of 340 ns and 920 ns³⁰.

Table II lists intensities of the fast emission component and of the total light intensity obtained in different studies with alkali PMTs, a solar-blind Cs-Te PMT and a TMAE gas photodetector. The measured photoelectron signal depends on many factors, such as the way crystal surface is treated, the wrapping material, the type of PMT photocathode, and how a crystal is coupled to a PMT. Also, the fast/slow photon ratio depends on particle type and is about 0.2-0.3 for gamma-rays and electrons. For alpha particle excitation the fast component is scarcely observed⁴⁰.

The importance of surface treatment, particularly polishing, on the amount of fast scintillation detected was reported in several studies^{32, 33, 48, 55-57}. Other studies stressed the importance of reflector around crystals^{33, 38, 56, 58, 59}. The best results were obtained with the teflon film. Teflon film, however, becomes semitransparent in contact with leaking coupling grease from the junction of the crystal and the PMT window. Silicon rubber gaskets were reportedly used to seal in the leakage³⁸. Also, standard teflon is known to be radiation soft when irradiated in air, and further studies are needed to confirm its applicability to the high total dose environment. A new radiation-hard teflon wrapping made of interlocking meshes of silicone rubber and PTFE was proposed²⁵. Also, optical coupling is sensitive to pressure⁶⁰. Using TFE teflon UV reflector and a 50%/50% mixture of RTV and Viscasil silicon oil produced best results in a PET detector⁶¹. RTV

especially for crystal lengths below 4 cm⁶⁵. Also, care must be taken when coupling a crystal to a PMT by choosing an appropriate coupling grease transmitting well below 200 nm and the layer must be made as thin as possible in order to minimize absorption of the fast component^{37, 52}. It was found that a 12.5 micron layer of a selected grease had good transmittance²⁹.

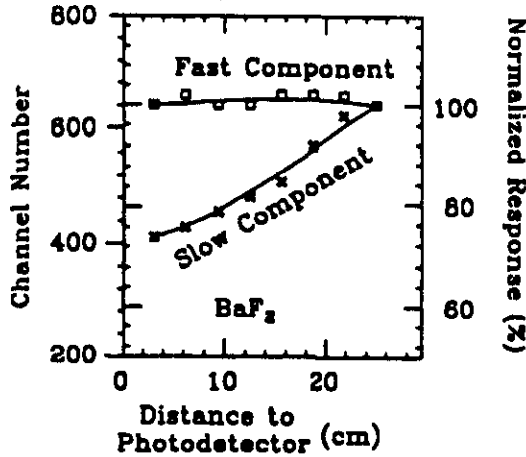


Figure 1.2.6: The longitudinal light collection response of BaF₂ crystals measured with a collimated ¹³⁷Cs source for aluminum wrapping^{23, 24}.

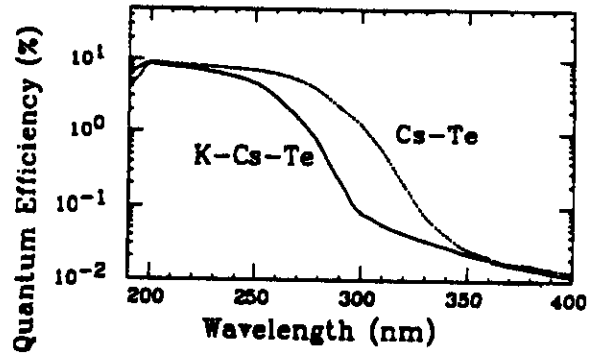


Figure 1.2.7: Quantum efficiency of a new K-Cs-Te photocathode as compared to a Cs-Te photocathode^{23, 24}.

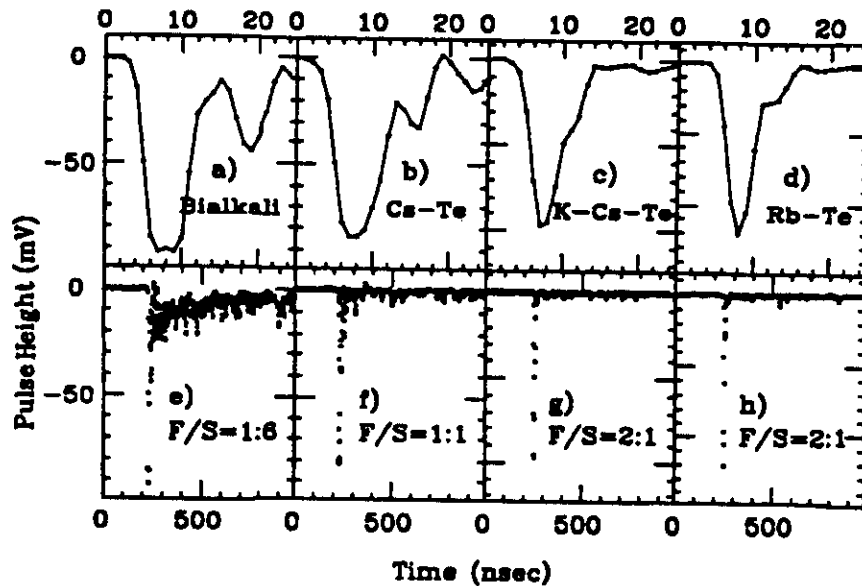


Figure 1.2.8: Scintillation light pulses and ratios of fast to slow components from pure barium fluoride crystal observed using PMTs with bi-alkali, Cs-Te, K-Cs-Te and Rb-Te photocathodes²⁵.

It is an obvious idea to limit the response of a photomultiplier, or photodetector in general, to a fast component of barium fluoride light by a proper choice of a solar blind photocathode. Already in one of the first papers following the discovery of the fast

The best selective photocathode known at present is the reflective photocathode of CsI with adsorbed layer of TMAE ^{68, 75} (figure I.2.10). A comparison of the photoelectron yield for an infinite TMAE gas layer and a CsI-TMAE photocathode is also shown ⁷⁴. Again, a serious question is a stability and ageing of such a photocathode in actual experimental conditions, including effects of gas impurities and ion production ^{72, 75}.

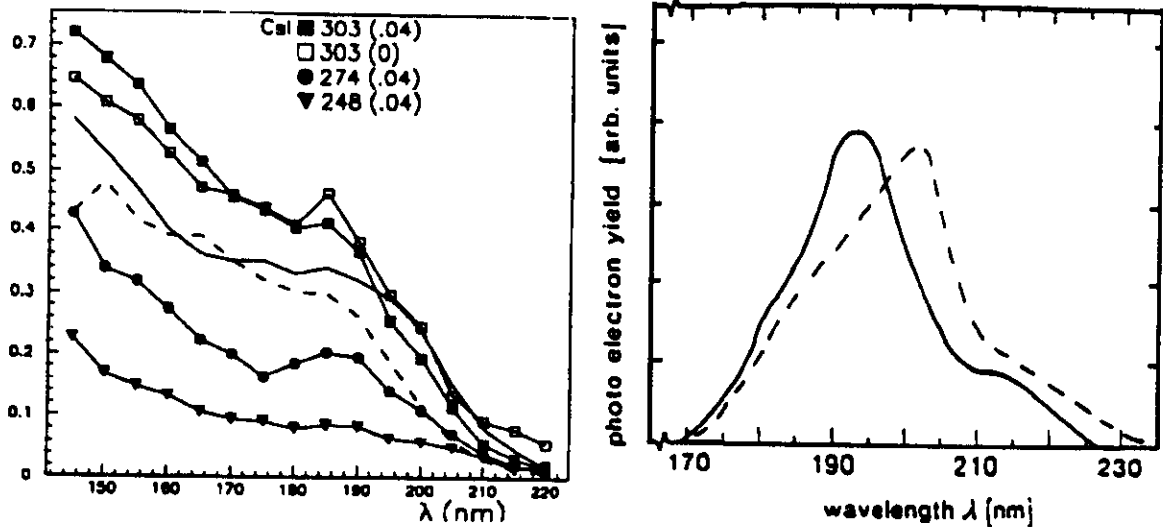


Figure I.2.10: Left: Quantum yield versus photon wavelength of the 500 nm thick CsI photocathode with solid, liquid, or adsorbed film layers of TMAE. For each curve the photocathode temperature is given in $^{\circ}\text{K}$ and TMAE partial pressure in Torr (in brackets); the solid line is for the TMAE gas, and the dashed line is for pure CsI ⁶⁸. Right: Comparison of the photoelectron yield for a TMAE gas photocathode (solid line, an infinite absorption thickness is assumed ⁴¹) and for a surface CsI-TMAE photocathode (dashed line) ⁷⁴.

A possible application for the gas-filled photodetectors in connection with barium fluoride is in the preshower counters where superior position resolution can be obtained ⁷⁶. Figure I.2.11 shows a design of the proposed preshower detector with a pad photocathode array coupled to a parallel plate avalanche chamber (PPAC) electron amplifier ⁷⁶.

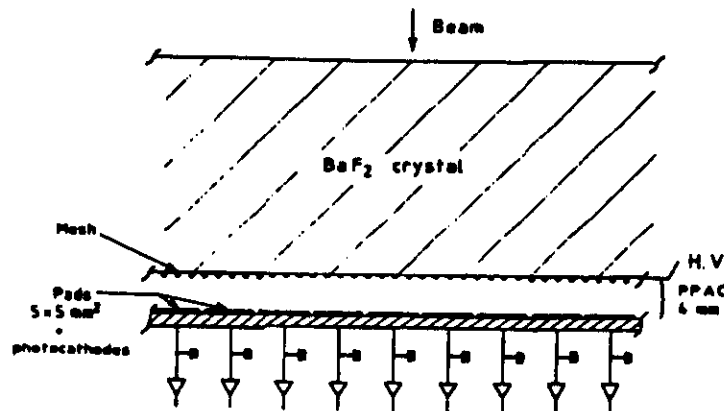


Figure I.2.11: Design of the BaF₂ preshower counter ⁷⁶.

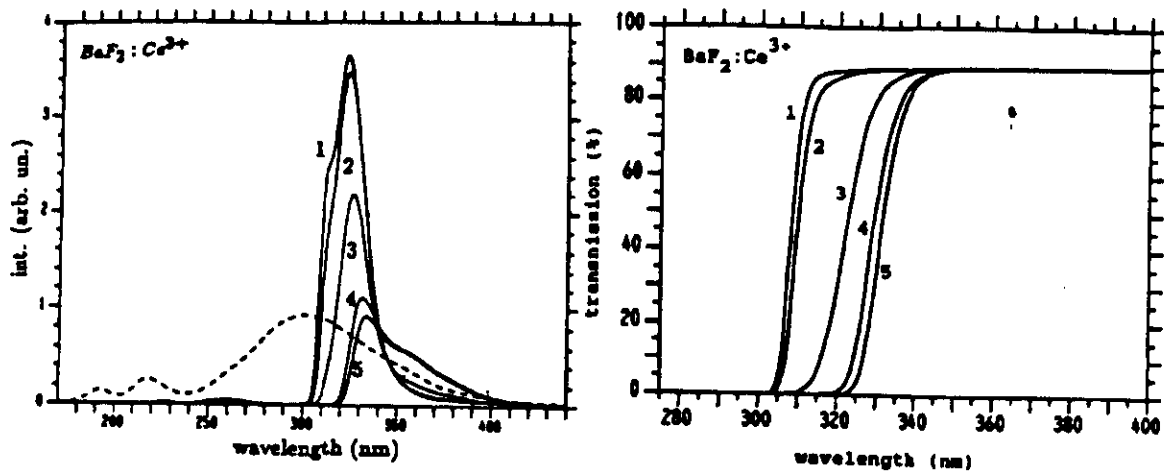


Figure I.2.12: X-ray induced emission spectra (left) and transmission curves of Ce doped 1" dia. x 1" BaF₂ crystals. Spectrum 1: 0.2 mol% Ce; 2: 0.3 mol%; 3: 0.5 mol%; 4: 0.8 mol%; 5: 1.0 mol% ⁸⁶. The dashed emission curve shows the emission spectrum of a pure BaF₂ 1" dia. x 1" crystal.

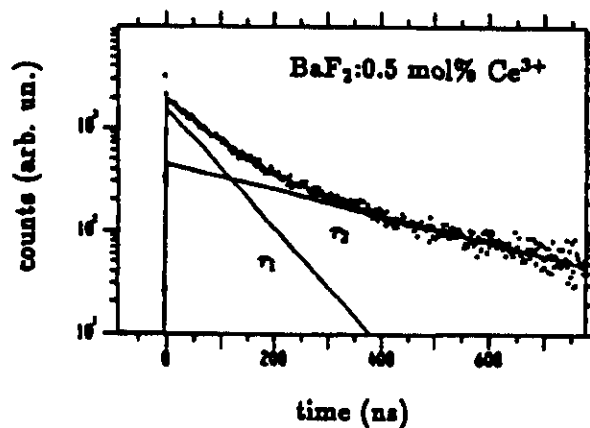


Figure I.2.13: Decay time spectrum of a BaF₂ crystal doped with 0.5 mol% cerium ⁸⁶. The decay time spectrum was fitted with two slow components: $\tau_1 = 75 \pm 4$ ns and $\tau_2 = 340 \pm 40$ ns.

The ratio of the relative intensities of the shorter to longer components is changing by almost a factor of 9 in the above range of doping levels, from 0.33 at 0.2 mol% to 2.8 at 1.0 mol%. This implies that even at 0.2 mol% the decay time is dominated by a decay component with a 210 ns decay constant. There is also a very slow emission with a decay time of about 0.2 ms. This component achieves maximum for Ce³⁺ concentrations of about 0.2 mol% and disappears for Ce³⁺ concentrations larger than 1 mol%. The photoelectron yields of doped crystals have values between those reported for BGO crystals and pure BaF₂ crystals and show a maximum for Ce³⁺ concentration near 0.2 mol% ⁸⁷ (figure I.2.14).

Light intensity of cerium doped barium fluoride is a slowly changing function of temperature depending on doping level ⁸⁷. For a 4.4 mol% cerium concentration the intensity drops only by 50% between room temperature and 200 °C ^{30, 83}.

The effect of La doping on the fast scintillation components is much smaller than that on the slow component. A suppression factor of 6 was obtained for the slow component by doping BaF₂ crystal with 1% lanthanum, accompanied by only a 10% reduction in the fast component intensity⁸⁹. The average decay time of the slow component decreases with increasing La³⁺ concentration (figure I.2.16). As an example, the decay time spectrum of a crystal doped with 2.37 mol% La³⁺ is shown⁸⁸. The suppression effect was attributed to the presence of interstitial F ions causing quenching of the slow luminescence by dissociation of self-trapped excitons. The inclusion of an additional quenching mechanism is consistent with the observed weaker temperature dependence for the lanthanum-doped samples⁸⁴. This implies that heating is less effective in suppressing the slow component in the doped material. The radiation hardness of the small lanthanum-doped BaF₂ samples was found not to be affected significantly up to at least 1MRad⁸⁴.

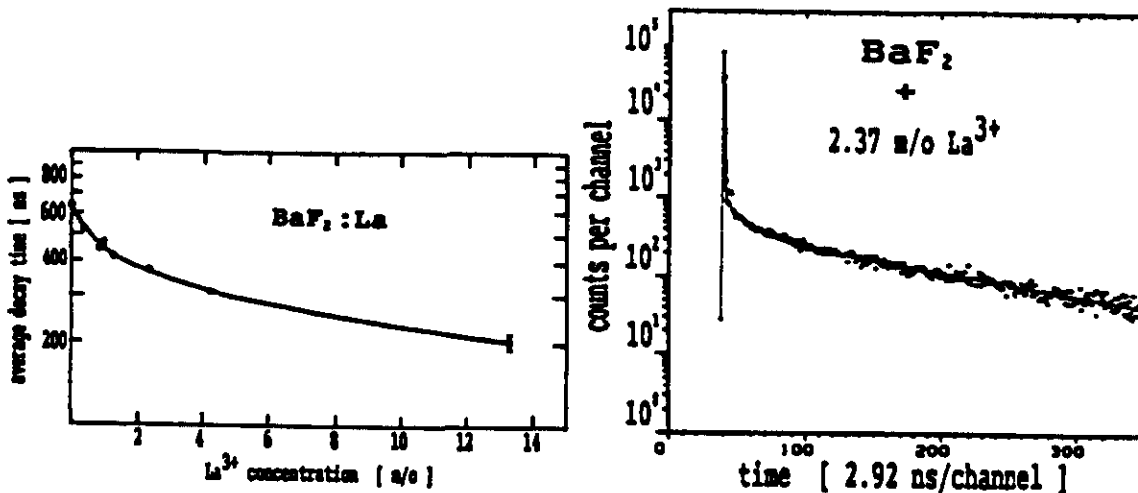


Figure I.2.16: Left: average decay time of the slow component of BaF₂:La³⁺ as a function of the La³⁺ concentration⁸⁹. Right: decay time spectrum for the luminescence of BaF₂ doped with 2.37 mol% La³⁺⁸⁸.

However, this method is only partially successful, and studies to find an appropriate dopant to obtain more significant improvement in the fast/slow ratio were proposed⁹⁰. Doping with trace amounts of transition or post-transition metal ions was proposed.

The suppression of the slow component might be achieved by a combination of doping with lanthanum and the use of a solar blind photocathode. A combination of Cs-Te photocathode and La-doping was shown to decrease the ratio fast/slow to 5:1³³. Figure I.2.17 shows emission spectra of pure and lanthanum-doped BaF₂ and quantum efficiencies of a regular alkali and a Cs-Te photocathodes.

Attempts to exploit the fast barium fluoride component went beyond using pure or doped crystals. A PMMA plastic scintillator doped with barium fluoride powder (70-86% by weight) was developed and its properties studied⁹¹⁻⁹⁴. Its operation is based again on the principle of wavelighting of the barium fluoride emission by dopants/dyes, but this time dissolved in the mixture of barium fluoride and plastic. The emission spectrum is

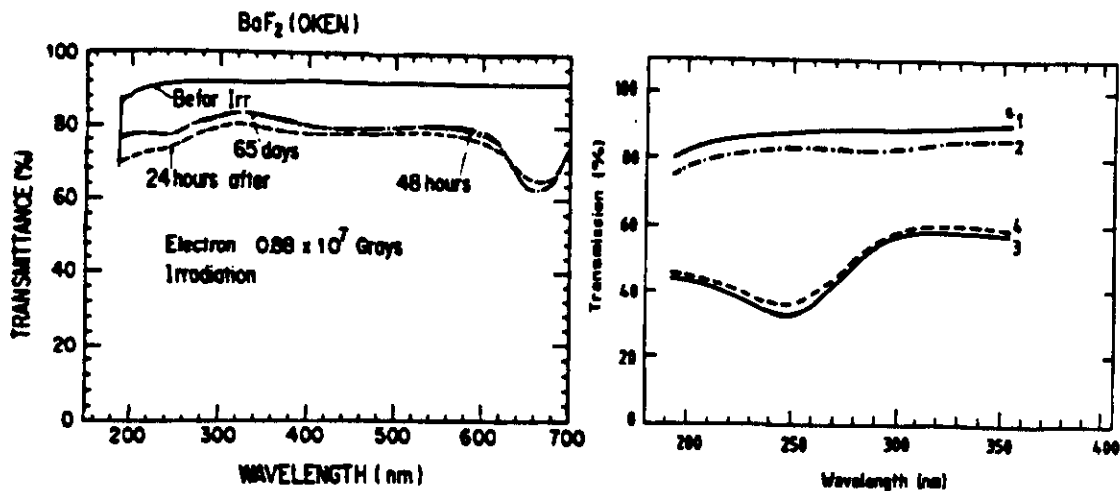


Figure I.2.18 Transmission of two crystals before and after irradiations and during recovery. A 1 mm thick sample at the left ⁹⁶ was irradiated to 88 Mrad with 2 MeV electrons. A transmission of a 5 cm sample at right ⁷⁶: before irradiation: 1; after 50 Mrad: 2; after 170 Mrad: 3; after three weeks recovery: 4.

On the other hand, not surprisingly, the crystals of a lesser quality were observed to be much more susceptible to radiation damage ^{24, 33, 34, 96, 99, 100}. The common underlying source of post-irradiation effects might be the presence of impurities or defects inside the crystal. It was suggested that radiation damage in BaF₂ is not caused by intrinsic color centers in the bulk material, but rather by externally introduced impurities ^{24, 34}. The observed saturation of radiation damage in the case of gamma-rays and neutrons supports this suggestion ¹⁰¹, but is not the only possible explanation. Figure I.2.19 ⁵⁷ shows almost no change in transmission up to a gamma dose of 10⁴ Rad, and a saturation in radiation-induced absorption at a dose of 10⁶ Rad. Small BaF₂ samples were irradiated up to a dose of ~620 MRad, and no change of the intensity in the fast component was detected. The samples were irradiated in sealed glass containers to avoid the effects of moisture. A very efficient and almost complete recovery of both transmission and scintillation output was stimulated by exposure to UV light from a mercury lamp. This result indicates that no permanent damage was produced in these crystals by irradiation. After a dose of 50 MRad the absorption length is still relatively long (~25 cm).

Defects and observed increased damage in the surface region due to surface treatment and/or water/oxygen absorption are also being investigated as possible contributing factors. The key issue is if large size crystals with low enough levels of impurities can be produced. Research both on chemical and other methods of material impurity analysis is currently underway, as well as investigations of the possible mechanisms responsible for color center formation ^{25, 33, 101}. For example, the absorption dip around 285 nm in transmittance of some 25 cm long crystals is attributed to cesium contamination. Another impurity identified to cause color center formation in BaF₂ is lead, manifesting itself in an

chemical groups OH⁻ and O₂⁻ produce wide absorption bands and substantially reduce the transmission of crystals. Strong absorption in the 190-250 nm region was induced in samples deliberately produced with a high oxygen content ¹⁰⁴. This is believed to be caused by O₂⁻ ions or ion pairs. Under irradiation the dissolved oxygen atoms or molecules will be transformed into oxygen ions, thus producing the absorption in the 190-250 nm region. The moisture from air leads to the appearance of a several micron thick surface layer. This is the reason why the transmittance of crystals kept in air deteriorates with time. Removal of moisture may be achieved by annealing @ ~300°C.

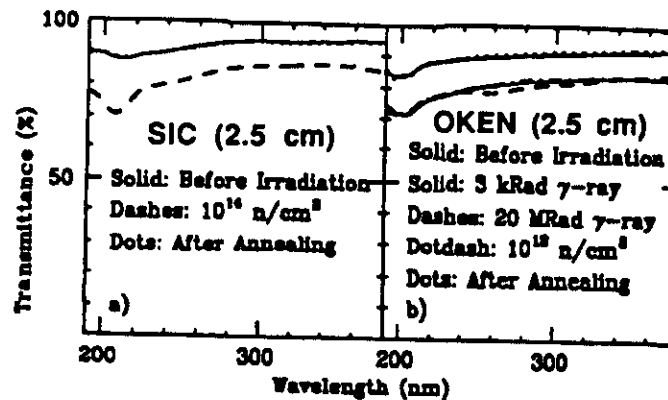


Figure I.2.20: Transmittances before and after irradiation showing recovery from neutron damage (a) and a typical saturation effect and recovery in the case of gamma damage (b) ²⁴.

It should be commented here, that the detected light output changes that cannot be explained by simple internal transmission losses do not necessarily mean that there is a decrease in the intrinsic scintillation yield. Changes in surface reflectivity, amplification of absorption losses due to multiple photon reflections in the crystal and, finally, absorption at the exit surface can contribute to the net effect of decrease in the light output. Determination of the possible impact of these phenomena is presently being studied through simulation programs ^{34, 101}. The above interpretation claiming that there is no damage to intrinsic scintillation yield is supported by the results of measurements of induced scintillation emissions in two 1" diameter x 1" long samples during irradiation. No change of emission intensity was observed up to 10⁶ Rad ³⁴. This confirms the result of the original measurement showing no damage to scintillation yield at a charged particle dose of 1.3 x 10⁷ Rad ⁵⁰ and the new results reported ⁵⁷.

In recent high dose-rate (3.4-3.8 x 10⁴ Rad/hr) gamma irradiation tests of 1 inch diameter and 1 inch long samples to about 5 Mrad, a strong post-irradiation afterglow phosphorescence was observed ³⁴. The emission, however, peaked at around 330 nm, well above the region where the solar blind photocathodes such as Cs-Te are sensitive. Also, the intensity of induced phosphorescence died away quickly with three time decay components in the range of 2-220 s. The longest component was of highest intensity. Some crystals showed signs of phosphorescence months after irradiation, proving that much longer phosphorescence components were also present. Exposure to roomlight or sunlight, or an increase in the crystal's temperature accelerates the deexcitation by

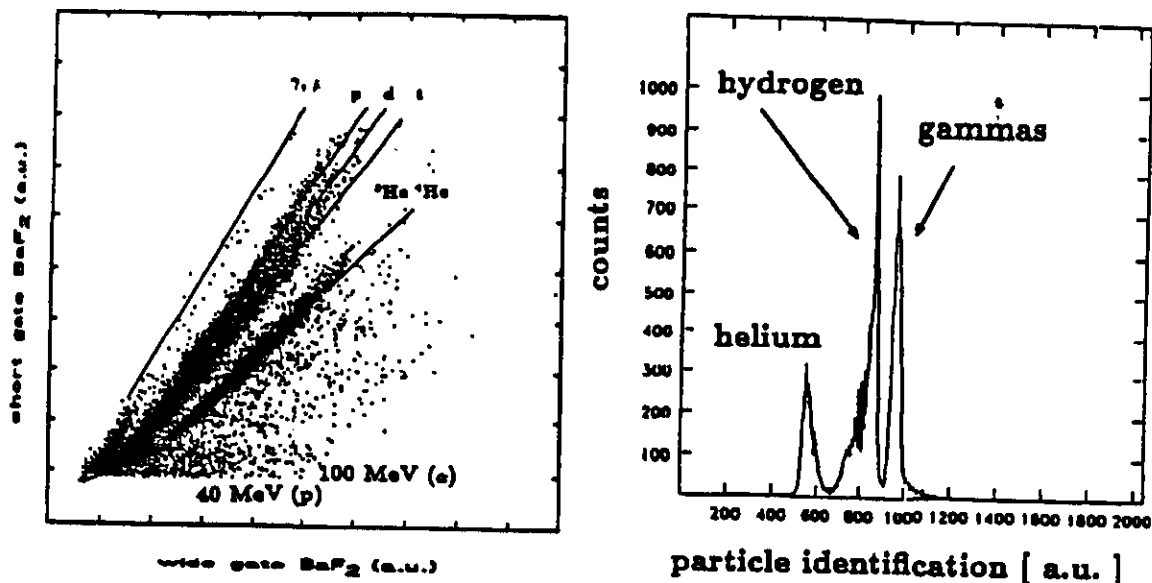


Figure I.2.21: Scatter plot of the fast scintillation component vs. the total light output (left). Projection of the separated particle lines after linearization (right) 22.

Time and energy response of BaF₂ to intermediate energy ions have been studied. Timing properties as good as for plastic scintillators were obtained ¹⁰⁹. The response to neutrons below 22 MeV was measured and a conclusion was reached that partial discrimination between neutrons and gammas was not possible in the energy range studied, but that it might be possible at higher neutron energies ¹¹⁰. It was also concluded that BaF₂ scintillators of a relatively large size are a favorable alternative to BGO for the detection of high-energy gamma-rays ¹¹¹. The superior timing properties of BaF₂ scintillators were found to be particularly suitable for in-beam gamma-ray spectroscopy ¹¹². Combined time-of-flight measurement and pulse shape analysis enabled separation of hard gamma photons with energies up to 130 MeV from charged particles and neutrons ¹⁰⁶. At these high photon energies detection and summing of the shower leakage in a ring of six hexagonal neighbouring modules significantly improved the energy resolution as compared to the resolution of a single module for photons of up to 50 MeV ¹¹³. Good agreements with Monte-Carlo simulations of gamma response were obtained ^{106, 113, 114}. The response function of a BaF₂ detector for electrons of energies 50-150 MeV was found to be in excellent agreement with computer simulations ¹¹⁵.

Three large size detectors have been built with BaF₂ crystals: the Strasbourg crystal castle ²⁰, the Karlsruhe 4 π detector ²¹ and the TAPS Darmstadt detector ^{22, 116}. The Strasbourg detector was the first large volume BaF₂ detector built with 74 hexagonal crystals arranged in several plane structures meant to achieve a high efficiency of gamma-ray detection. The Karlsruhe 4 π detector, consisting of 42 hexagonal 15 cm long crystals, was found to have a nearly 100% efficiency for gamma-rays of up to 10 MeV. It was built for precise measurements of neutron capture cross sections in the neutron energy range of 3 to 200 keV. The overall achieved time resolution was 500 ps and the peak efficiency was

comparators was demonstrated ¹²⁰. The main advantage of these new circuits is a substantially reduced walk of ± 20 psec for a dynamic range of 100:1.

1.2.7. Other Applications

The potential of BaF₂ for positron emission tomography (PET) was acknowledged immediately after the discovery of its fast component ^{36, 37, 48, 121, 122}, and BaF₂ tomographs were built ^{61, 123-126} since they could provide time-of-flight (TOF) information in addition to projection measurements. This led to an improved signal-to-noise ratio. A special version of a PET camera based on a BaF₂ scintillator coupled to a low-pressure MWPC filled with TMAE gas photocathode was developed ^{47, 53, 127-133}. The capabilities of this detector include over 40% quantum efficiency of detection of annihilation gammas for a 50 mm thick BaF₂ crystal, 5.6 mm FWHM spatial resolution, and a 2.4 ns time resolution ¹²⁷. A version of this detector to operate at atmospheric pressure and with a CsI photocathode is under development ¹³⁴. BaF₂ was also recently considered for well logging applications, but it was found that the intensity of its fast component is too weak ^{30, 135}.

I.3. Cerium Fluoride

Cerium Fluoride (CeF₃) with its two originally reported ^{136, 137} fast scintillation components of 2-5 nsec (310 nm) and 30 nsec (340 nm) (figure I.3.1), no slow component, and light output equal to one-half of that from pure CsI (and 4-5% of that of NaI(Tl)) is intensively studied for LHC ⁶⁻⁸. Besides the applications in high energy and nuclear physics, CeF₃ is also proposed for positron emission tomography.

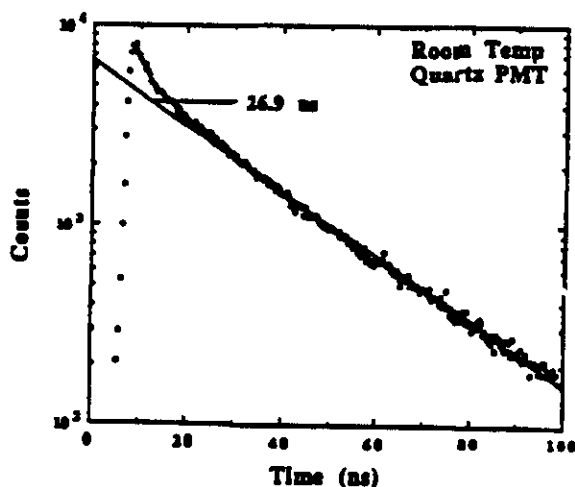


Figure I.3.1: Scintillation decay curve with a quartz PMT at room temperature of CeF₃. Scintillation was excited with gamma-rays from ²²Na ¹³⁷.

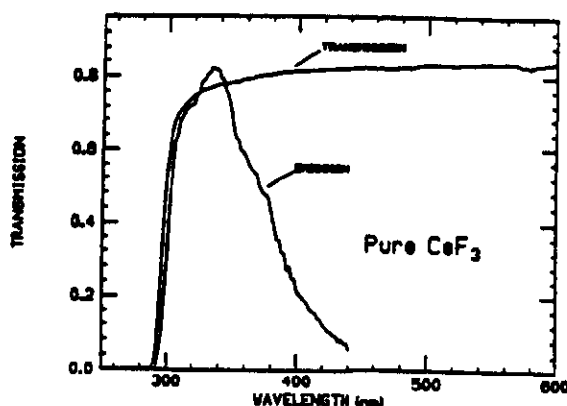


Figure I.3.2: Emission spectrum and transmission as a function of wavelength at room temperature. Emission excited with 254 nm UV light ¹³⁷

CeF₃ is 25% more dense (6.16 g/cm³) than BaF₂ with the advantage of about 20% shorter radiation length (1.68 cm) and about 25% smaller Moliere radius (2.63 cm). Also its

was no significant effect of irradiation on the emission characteristics even after a dose of 10^8 Rads.

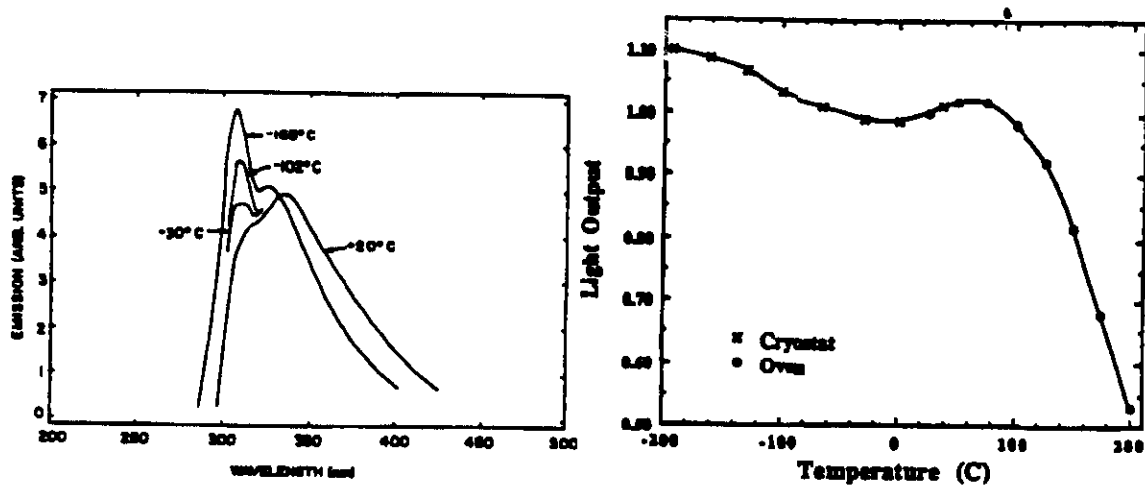


Figure 1.3.3: Emission spectra of CeF₃ excited with 511 keV photons from a ²²Na source at different temperatures 137.

Figure 1.3.4: Light output of CeF₃ as a function of temperature 137.

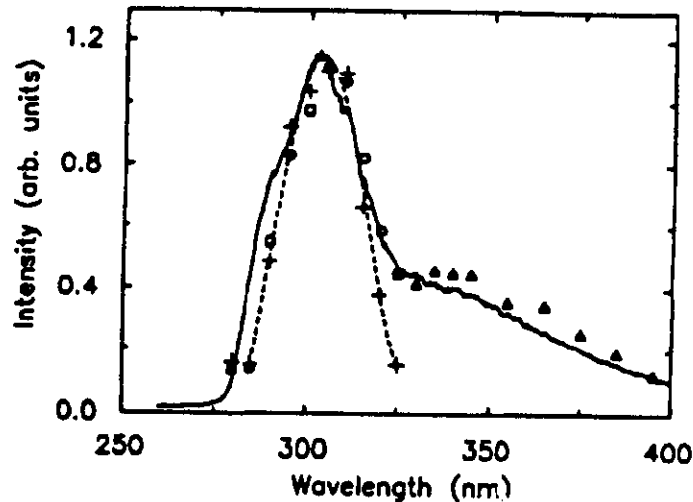


Figure 1.3.5: Emission spectra of CeF₃ excited with 270 nm UV laser pulses (solid line) and under Ru/Rh beta/gamma source excitation for the three identified decay components (+: 2.1 ns, o: 17.3 ns, and Δ: 32.6 ns). Broken line is a polynomial fit to the 2.1 ns component 143.

The radiation damaged transmission recovered with an exponential time constant of about 40 days. No effects of accelerated recovery due to exposure to sunlight were observed. These results place CeF₃ just next to BaF₂ in radiation resistance. Preliminary irradiation of a 8 cm long crystal to 100 KRad showed positional variation of color center formation due to changing gradient of impurity concentration in the melt⁸. In some parts of the crystal the damage was very severe, but at one end the damage level was acceptable. Characterisation

neutron thermalizing hydrogen-rich material is present. Its applicability as a gamma-ray detector for nuclear well logging applications was evaluated and found promising ¹⁵³.

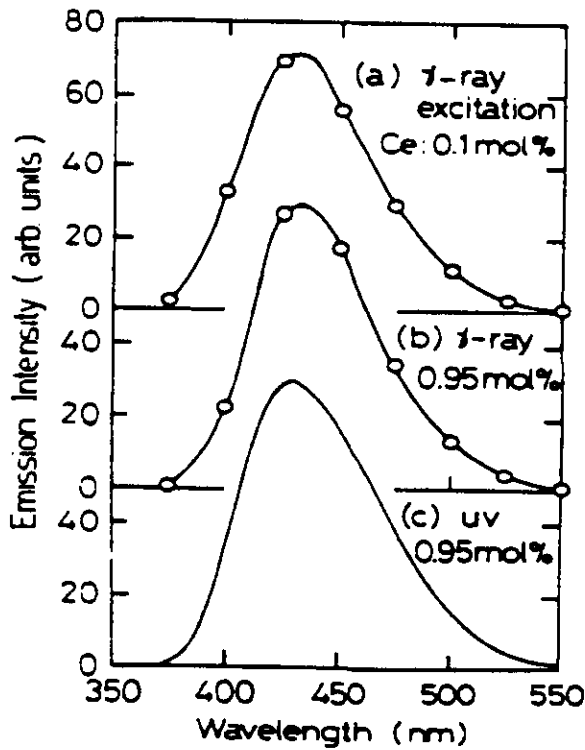


Figure I.4.1: Emission spectra of GSO(Ce) with a Ce concentration of 0.1 mol% (a) and 0.95 mol% (b) when excited with 662 keV gamma-rays @ 295 °K, and with 0.95 mol% when excited by UV photons (c) ¹⁴⁷.

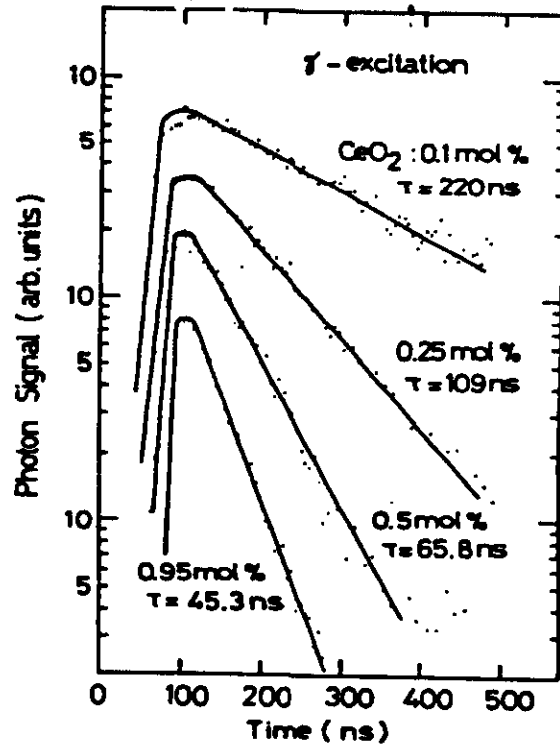


Figure I.4.2: Decay curves for GSO(Ce) with various Ce concentrations excited by ¹³⁷Cs gamma-rays ¹⁵¹.

Fast rise times of 3 ns and fast decay constants down to 30-60 ns were observed ¹⁵¹ (figure I.4.2), depending on the Ce concentration and temperature, together with slow decay times up to 2 μs ^{147, 153}. Figure I.4.3 shows scintillation decay of a 2 cm x 2 cm x 2 cm GSO crystal doped with 0.5 mol% cerium ^{153, 154}. A fit was made to the experimental spectrum with the sum of two exponential terms with decay constants (and fractions of total scintillation light) of 57 ns (85-90%) and 600 ns (10-15%). The time constants of both decay components are strongly dependent on the concentration of the cerium dopant (Table III). The light output is greatest for the 0.5 mol% doping level and decreases for both higher and lower concentrations ¹⁵¹. About 10-15% of the total scintillation output is contained in the slow component. Due to the slow component, ADC integration gates with widths of up to 500 ns had to be used to collect light.

It is interesting to note that with 5 mol% of cerium activator, the slow component's decay time decreases to 70 ns. Both light output and decay times decrease monotonically with increasing temperature (figure I.4.5) ¹⁵³. Over the temperature range of 20-170 °C the light loss is comparable to the loss for NaI(Tl) and is equal to about 40% @ 150 °C. The

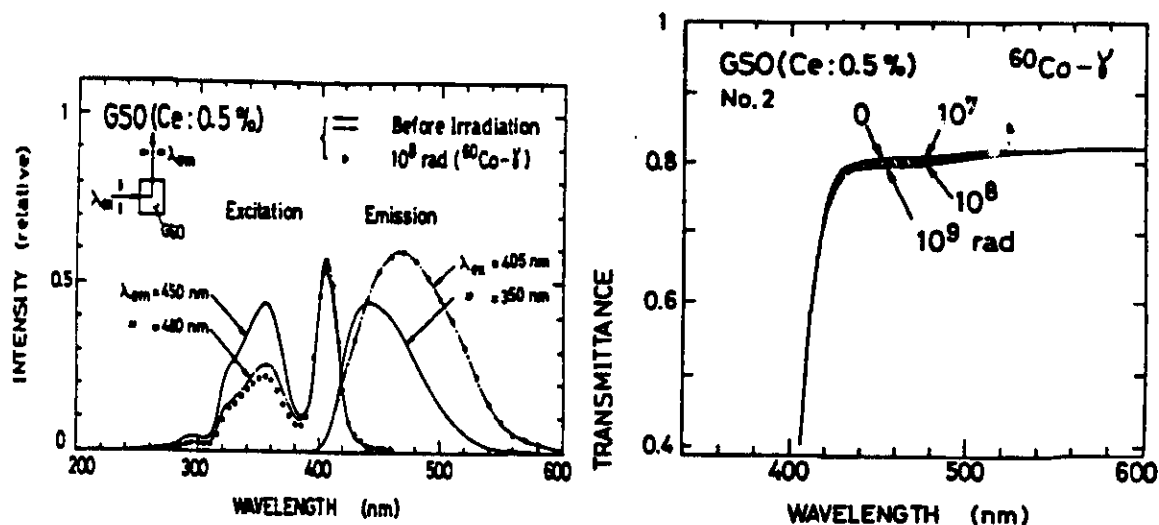


Figure 1.4.6: Excitation-emission and transmission spectra of GSO(Ce) samples doped with 0.5 mol% of Ce measured before and after ⁶⁰Co gamma irradiations to 10⁸-10⁹ Rad. Transmission measured across a 1 cm thickness ¹⁵⁰.

Disadvantages of GSO are (1) its high melting point (1900 °C) and (2) the high segregation factor of cerium in this matrix resulting in a low pulling rate of 1-2 mm/hour ⁸.

In many cerium-doped crystal scintillators there are means to alter the matrix with Li or Ni resulting in a reduction of scintillation lifetime. But, quite possibly, this might have an adverse impact on radiation resistance of the new material.

1.5. Pure CsI

1.5.1. Properties

Pure CsI, whose emission was already observed in the 1960s, re-emerged recently as an attractive candidate with superior mechanical properties to those of BaF₂ and easier to detect scintillation light in the longer wavelength region ¹⁵⁵. It has a dominant emission band occurring between 305-320 nm ¹⁵⁶ (figure 1.5.1) of scintillation light with fast 10, 23 and 36 ns decay constants originally reported ¹⁵⁵.

CsI is only slightly hygroscopic, with a surface weakly sensitive to exposure to humidity. It is however highly shock resistant, thermally stable, and easy to process. CsI is not susceptible to cleavage or cracking under mechanical or thermal stress. In the more recent studies two components of about 6-7 ns and 29-30 ns ¹⁵⁷, and 2.1 ns (35%) and 21.7 ns (65%) according to a different study ¹⁵⁸, were identified. A slower 1 μs component associated with lattice defects and centered at 450 nm was also seen ¹⁵⁸ (figure 1.5.2). The fast/total ratio depends on the purity of material and the highest attainable value is about 0.8 ¹⁵⁷. In a new study ¹⁵⁹ decay time measurements were made on pure CsI scintillators prepared by different methods. The main conclusion of that study was that the presence or absence of the slow component was strongly correlated with the production

than the fast one, and will cause less pileup at high rates. The scintillation mechanism of the fast band at 315 nm is explained in terms of the radiative decay of self-trapped excitons ^{158, 160}. The slow 450 nm component is attributed to the presence of vacancies and other defects ^{158, 160}. Chemically pure crystals with as little defects as possible are therefore required. The intensity of the slow component, the shape of the emission spectrum and transmission properties were shown to be at least partly related to the level of impurities, such as Tl, in the crystal ¹⁵⁶.

A potentially serious drawback of pure CsI is the steep dependence of its light yield on temperature, requiring precise temperature monitoring in large detector systems (figure I.5.3) ¹⁵⁷. Decay constants of the fast (7 ns and 29 ns) components of CsI scintillation light increase with decreasing temperature. At -190 °C they are 180 ns and 320 ns, respectively. This is accompanied by an increase in the total light output by a factor of 6. Also, a shift in emission spectrum to longer wavelength occurs at lower temperatures ^{157, 162}. Figure I.5.1 shows a shift in the peak emission from 310 nm at room temperature to 340 nm at liquid nitrogen temperature ¹⁵⁷.

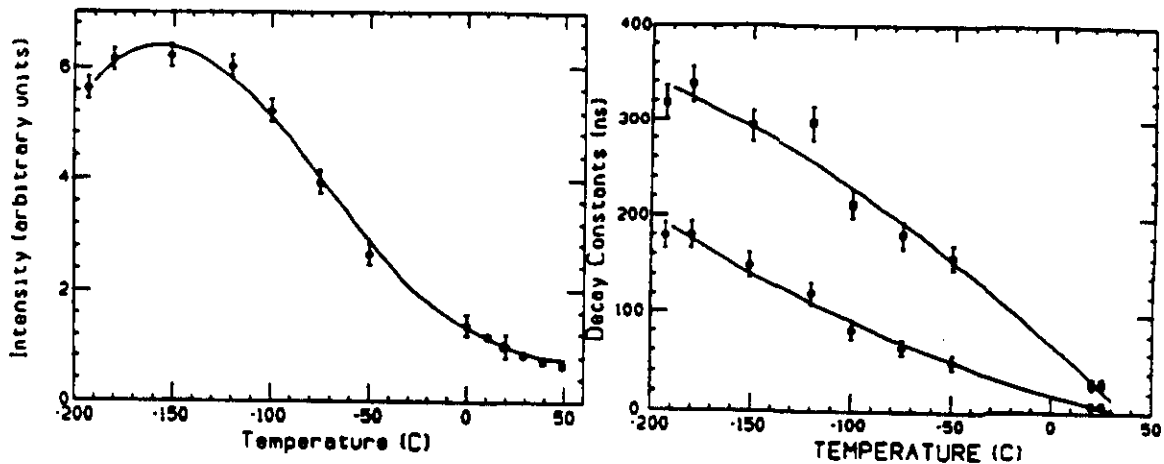


Figure I.5.3: Variation in the light intensity of the fast light output (left) and in the decay constants (right) of the two fast components in undoped CsI as a function of temperature ¹⁵⁷.

CsI can be grown like CsI(Tl) into very large ingots. Large detectors such as the 7800 crystals CLEO II ^{163, 164} and Crystal Barrel were built with CsI(Tl). A high-resolution, large-acceptance spectrometer for neutral mesons was constructed at LAMPF with two pure CsI calorimeters, each made with 60 large 4" x 4" x 13.5" long crystals ¹⁶⁵. The same developed techniques can be used to produce pure CsI. New improved purification and production processes developed for CsI(Tl) resulting in considerably better uniformity of scintillation efficiency ¹⁶⁶ help with pure CsI production. Large 30 cm long good quality crystals became recently available ^{167, 168}. Fast light yield of 250-300 pe's per MeV was measured in these crystals with a 100 ns effective ADC gate (figure I.5.4). Total light output was measured with a 1 μ s gate.

al. 157, 167, however, show that it can be made radiation resistant to at least a fraction of a megarad of a ^{60}Co gamma dose. Figure I.5.5 shows the radiation induced absorption during irradiation and recovery for one of the best among the tested samples. The samples were irradiated at a dose rate of 3.4×10^4 Rad/hr in a dry nitrogen atmosphere to prevent any surface deterioration due to moisture during the exposure.

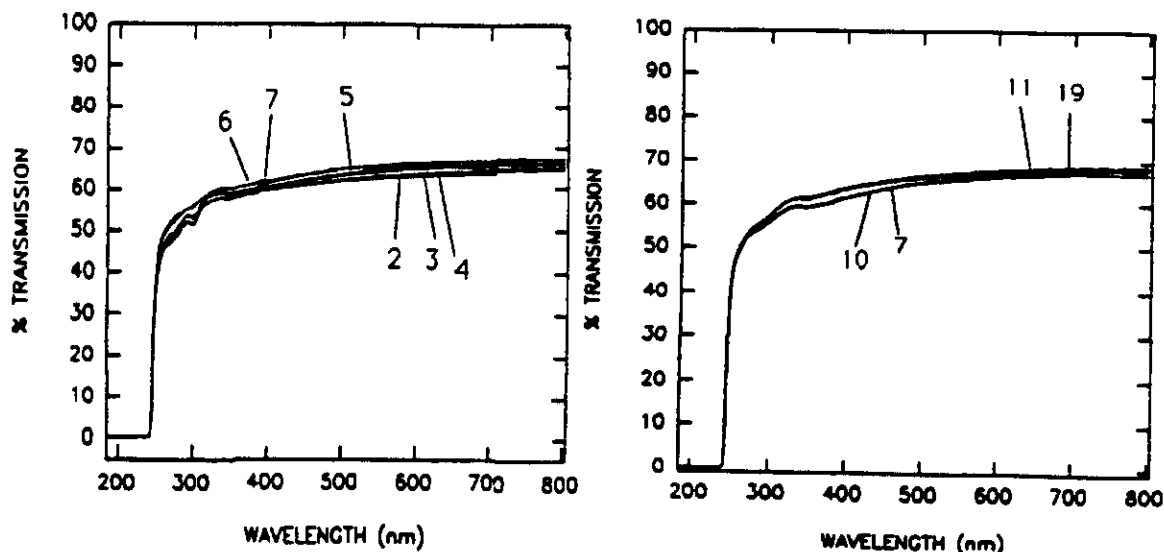


Figure I.5.5: Transmission vs. wavelength for the undoped Quartz & Silice 1" dia. x 1" long CsI sample: (2) 10^3 Rad, (3) 10^4 Rad, (4) 6×10^4 Rad, (5) 2.6×10^5 Rad, (6) 9.0×10^5 , (7) 4.2×10^6 Rad, (8) 7 hours after 4.2×10^6 , (10) after 54 hours, (11) after 20 days, (19) after 26 days plus 63.5 minute exposure to UV light 167.

Decrease in the light output of the same Quartz & Silice 1" dia. and 1" long sample with a gamma dose is shown in figure I.5.6. A $\sim 35\%$ loss of light output is seen. This loss exceeds what would be expected from loss in transmission only (which is very small in this sample; see figure I.5.5). Other 1" dia. x 1" long tested samples have shown worse performances, and large sample to sample variations in transmission and light output damage were measured.

Scintillation emission spectra measured during gamma irradiation have shown some increase in the spectral region of the slow component, while little change occurred in the region of the fast emission (figure I.5.7). Within experimental errors the intensity of the fast component did not change up to the highest doses used. Hence, the observed changes in light output cannot be accounted for by the combined measured effect of the losses in transmission and in light yield. One of the investigated possibilities is the potential role played by radiation effects near or at the surface, which could change light collection efficiency. A slow recovery with time was seen in all irradiated samples. Exposure to UV light from a mercury lamp did not induce acceleration of recovery. All five samples of a 2.54 cm diameter and 2.54 cm long used in the study have shown a prominent absorption band at 800 nm and several bands in the 250-500 nm region. No recovery was observed in the latter region for this sample, while a substantial recovery was shown for the 800 nm

A phosphorescence emission was observed in the CsI crystals immediately after irradiation ¹⁶⁷. Several decay constants in the range of many seconds were identified, and some residual emission was detected in samples even several days later.

Another study of radioluminescence and radiation damage in single crystals and in polycrystal CsI thin infrared windows was performed with 100 kRad 14 ms wide reactor pulses with 5 kRad neutron and 95 kRad gamma components ¹⁷⁰. After radiation doses of more than 2 MRad the radioluminescent intensity in the visible range decreased to about 60-70% of the pre-irradiation value and then recovered completely after bakeout at 150 °C. Apparently the quenching centers that were at the origin of the decrease of the emission have been annealed. Heat treatment of one non-irradiated pure CsI crystal at a higher temperature of 550 °C led to cloudy appearance, lowered intensity of the fast component, and longer wavelength emission bands extending from 350 nm to 550 nm ¹⁵⁶.

Interestingly, new samples of CsI doped with thallium were also found to be radiation hard ^{167, 171}. This indicates that impurities in the meltstock rather than thallium were then responsible for the observed radiation damage of CsI(Tl), already with doses of under a kilorad ^{169, 172-174}. Actually, thallium is expected to "protect" material against radiation damage by "scavenging free carriers before they can find a more damaging site" ¹⁷⁵. Impurities such as Rb, K, Na and Ba were found in a sample damaged by a ⁶⁰Co gamma dose of less than a 1 kRad, in contrast to other 1 cm³ samples which have displayed good radiation resistance up to the doses of over 50 kRad ¹⁷¹. An interesting effect was observed when comparing radiation resistance of two samples cut from the same boule. The sample cut from the first grown part of the ingot (bottom) was much more radiation hard than the sample from the top, pointing to the accumulation of impurities in the top part of the ingot grown by the vertical Bridgeman method. A chemical analysis has confirmed a higher concentration of impurities (Fe, Rb and Ba) in the top sample. No difference in radiation resistance was obtained by varying Tl content from 0.01% to 0.6%, proving that impurities and not thallium are responsible for radiation damage in CsI(Tl) crystals.

In a study of undoped (pure) CsI crystals a correlation was shown to exist between the light yield in the fast component and the vertical position in the ingot (grown by the Stockbarger process) from which the sample was taken ¹⁷⁶. A continuous decrease of the fast component and increase in the concentration of impurities with height were found.

One can point out to a similar experience with different samples of BaF₂ where contradictory radiation damage results were encountered until the role of relevant impurities and defects became more clear (the studies are continuing) and production of crystals of improved quality was made possible. This problem is presently further compounded by the fact that radiation damage tests are often done with small, better-than-average quality samples, and the predictions to the large actual-size samples are risky, and usually lead to an underestimation of the expected damage.

In general one would expect pure CsI crystals to be radiation hard. If proven, CsI would be a natural candidate for a B-Factory electromagnetic calorimeter ¹⁷⁷. Also, being faster than the thallium doped CsI(Tl), it should be a better solution than the latter choice proposed for a tau-charm factory electromagnetic calorimeter ¹⁷⁸. It was also selected as an

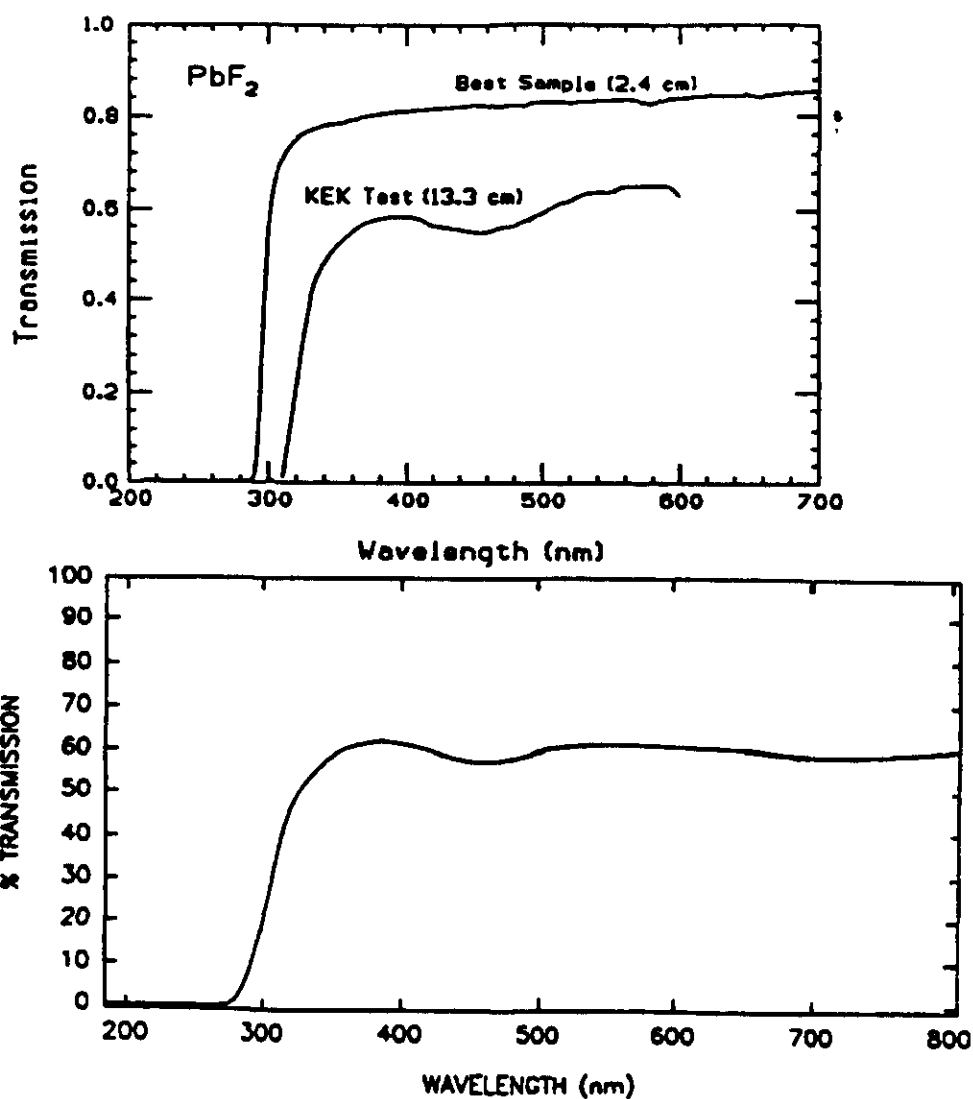


Figure I.6.1: Transmission as a function of wavelength of a small good quality sample and a 13.3 cm long KEK crystal (upper spectra, adapted from ref. 188), and of the new 17.5 cm sample tested 190 (lower spectrum). The curves shown have not been corrected for the ~17% loss due to reflections from the two end surfaces.

Doped with some fast scintillators such as TbF_3 , the ratio of the Cherenkov to the scintillation signal can be used to correct the visible hadron energy on an event by event basis 187. There are plans to dope this crystal with other cations and to produce more complex structures such as CsPbF_3 and $\text{Pb}_2(\text{Zn,Th})\text{F}_6$, which could be expected to show some scintillation 8. Breaking the local symmetry (believed to be the reason for the luminescence to be hidden) of the Pb^{2+} ion in the fluoride lattice is expected to produce a scintillating material 8. Other heavy crystals such as CdF_2 ($\rho = 6.33 \text{ g/cm}^3$), BaYb_2F_8 ($\rho = 6.99 \text{ g/cm}^3$) and YbF_3 ($\rho = 8.17 \text{ g/cm}^3$) are studied as scintillator hosts 8, 146. It was

Some residual permanent damage at the shortest wavelength remained in the sample irradiated to 4×10^6 Rad. In another measurement it was reported that a rather poor quality 1 cm thick sample, made from 98% purity raw material, showed effects of radiation damage after a ^{60}Co gamma dose of 10^4 Rad ¹⁴⁵. The research on this question continues. In figure I.6.3 the result of an irradiation test to 1.4 MRad with one of the new crystals of improved quality is shown ¹⁹⁰. The radiation resistance has significantly improved as compared to older samples. Except for the study of impurities responsible for the damage, it would be interesting to find an additive that would make PbF_2 more radiation-hard, much like different oxide dopants were found to suppress the production of color centers in lead glass ^{191, 192}. It was suggested that in order to improve radiation properties of PbF_2 , some metal fluorides of Li, Na, K, etc. may be used as additives ¹⁴⁶.

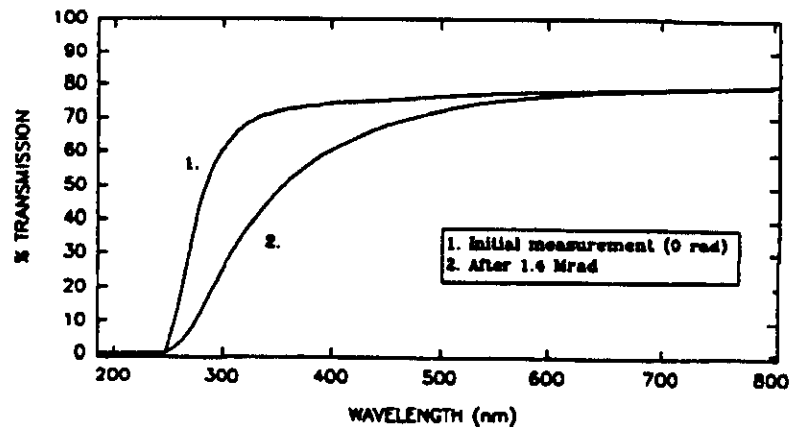


Figure I.6.3: Transmission spectra before and after a 1.4 MRad gamma irradiation of a 1" dia. x 1" long PbF_2 sample ¹⁹⁰.

The first batch of 20 radiation length long PbF_2 crystals were recently produced and are undergoing tests ¹⁹⁰ but the feasibility of production of large quantities of good quality crystals has yet to be demonstrated.

I.7. Brief discussion of some other materials

The search for new scintillating materials accelerates ^{9-12, 186, 193}. Blasse ¹⁸⁶ has critically reviewed some of the efforts. For example, he has pointed out that lead carbonate (PbCO_3) and many other studied heavy lead-based materials, such as PbF_2 , PbCl_2 , PbBr_2 and PbWO_4 were found to have their luminescence quenched at room temperature, and therefore were not good candidates for scintillators. According to Blasse new and potentially interesting scintillating materials include ZnGa_2O_4 , and several bismuth, gadolinium, barium and lead compounds. The main conclusion of his report is that the present level of understanding of the properties of luminescent materials can be used in order to search for new scintillators in a much more efficient way. At the present time there exists no fundamental approach in the search for new scintillating materials which would

A heavy material tested for a Cherenkov radiator is BaYb_2F_8 . It has a density of 6.99 g/cm^3 , and was shown to have good radiation resistance up to 10^7 Rad ¹⁴⁶. BaYb_2F_8 and other heavy crystals such as CdF_2 (6.33 g/cm^3) and YbF_3 (8.17 g/cm^3) are studied as possible scintillator hosts ⁸.

Lead carbonate (PbCO_3), a heavy (6.6 g/cm^3) scintillator was recently studied ²⁰⁷. Its scintillation light output is temperature dependent and has many decay components from 3.9 ns up to $1.4 \mu\text{s}$ at room temperature. Following the rediscovery of lead carbonate, a report appeared on a naturally occurring lead sulfate (PbSO_4) in the form of anglesite ¹⁹⁹. In a new study of lead sulfate samples it was measured that its emission, peaking at 335 nm , has two fast decay components of about 1.8 ns (5%), 19 ns (36%) but also long components with decay times of 95 ns (36%) and 425 ns (23%) ²⁰⁰. The slow component is the dominant one (about 60% of the total light output). Lead sulfate has a density of 6.4 g/cm^3 , and is not affected by air or moisture. It is, however, difficult to grow because it decomposes when heated. As a result of this good quality synthetic crystals are still not available at this time.

Yet another interesting development is the study of a new crystal scintillator with an unusually long wavelength of emission. CdS has an intense red emission between 600 and 800 nm ¹⁹⁷. In a preliminary study about 10^4 photoelectrons per MeV were detected when the scintillator was coupled to a silicon photodiode ¹⁹⁷. The material is hard and non-hygroscopic and has a density of 4.8 g/cm^3 . It could be expected to be radiation hard due to a long wavelength emission bypassing the usual absorption region caused by color centers. However, a serious disadvantage of this scintillator is its extremely long decay time (amounting to about $4 \mu\text{s}$).

YAlO_3

A promising new material is cerium doped yttrium aluminate ($\text{YAlO}_3(\text{Ce})$ or $\text{YAP}(\text{Ce})$) ^{8, 146, 201, 202}. It has a high relative light yield of about 2.5 times that of BGO or 30-40% that of $\text{NaI}(\text{Tl})$, a density of 5.35 g/cm^3 , is not hygroscopic, and was measured to have fast emission with a 15-30 ns decay constant as obtained in different studies. Figure I.7.1 shows absorption and luminescence of a 1 mm thick YAlO_3 crystal doped with 0.1% by weight of cerium ²⁰¹. The measured luminescence band at 347 nm is attributed to a $5d - 4f$ transition in Ce^{3+} . The scintillation decay spectrum for ^{137}Cs gamma-ray excitation is shown for the same samples, with a single 27 ns exponential component. Single-exponentiality of the decay demonstrates the absence of quenching centers in the tested samples. In addition to the fast component of 31 ns (98%), a second slow component of 246 ns (2%) was also seen ²⁰². The dependence of the light output normalized to $\text{NaI}(\text{Tl})$ and the decay constant on cerium doping level is presented in figure I.7.2. Decay time depends only weakly on cerium amounts above the 0.2% point (by weight).

Yttrium aluminate was also reported in a recent preliminary study to be very radiation hard ¹⁴⁶. In figure I.7.3 the transmission spectra of a 4 mm thick YAlO_3 sample doped with 0.6 mol% cerium measured before and after a ^{60}Co gamma dose of 10^8 Rad are shown. To increase crystal density a program was started to substitute yttrium with ytterbium or other isoelectronic cations ⁸.

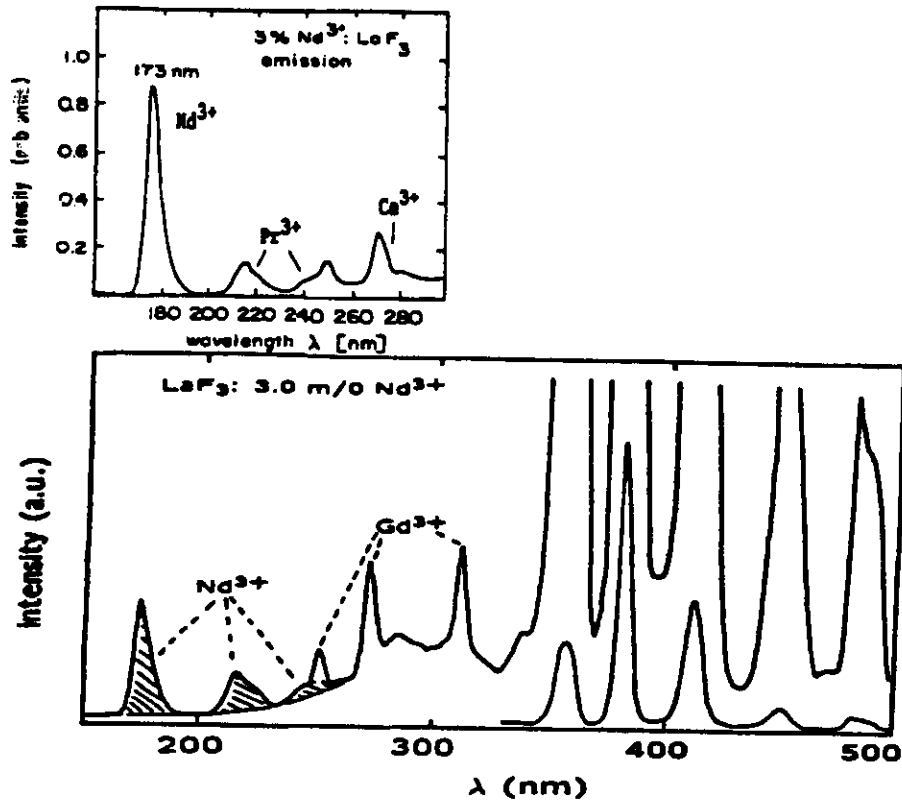


Figure I.7.4: Scintillation emission spectra of $\text{LaF}_3:\text{Nd}^{3+}$ (3 mol%) when excited with < 35 keV X-rays. (Upper spectrum from refs. 89, 203, see also correction 204; lower spectrum from ref. 205). Two intensity scales, different by a factor 25, were used in the lower spectrum in the region between 350nm and 500 nm.

The intensity of this band, originating from the fast allowed $5d - 4f$ dipole transition (of the same type as observed in the cerium-doped scintillators such as yttrium aluminate), increases with the rise (up to 12 mol%) of the Nd concentration. Presently available samples have contaminants such as Ce, Gd, and Pr, contributing to the emission spectrum and to absorption at wavelengths below 200 nm. At longer wavelengths there are also strong emission lines for 357 nm, 382 nm, 414 nm, and 448 nm from much slower (decay times of the order of milliseconds) $4f - 4f$ transitions in Nd^{3+} (figure I.7.). As in the case of BaF_2 , a selectively sensitive photodetector must be used to exploit the fast component only. An example is a PMT or a gas electron multiplier with a CsI photocathode. The samples used in a preliminary test with a TMAE gas photocathode have all shown a very low yield, at least a factor 10 lower than for BaF_2 ⁵³. It is possible that this poor performance was due to impurities in the samples. It was also reported that it is technically more difficult to grow LaF_3 crystals than BaF_2 crystals⁵³.

A similar crystal, $\text{LiYF}_4:\text{Nd}^{3+}$, has comparable light output to $\text{LaF}_3:\text{Nd}^{3+}$ with the 184 nm emission line corresponding to the 173 nm line in $\text{LaF}_3:\text{Nd}^{3+}$ ¹⁰.

Attempts with cerium-doped lanthanum fluoride have not resulted in a better, more efficient, or appreciably faster scintillator than pure CeF_3 ²⁰⁶.

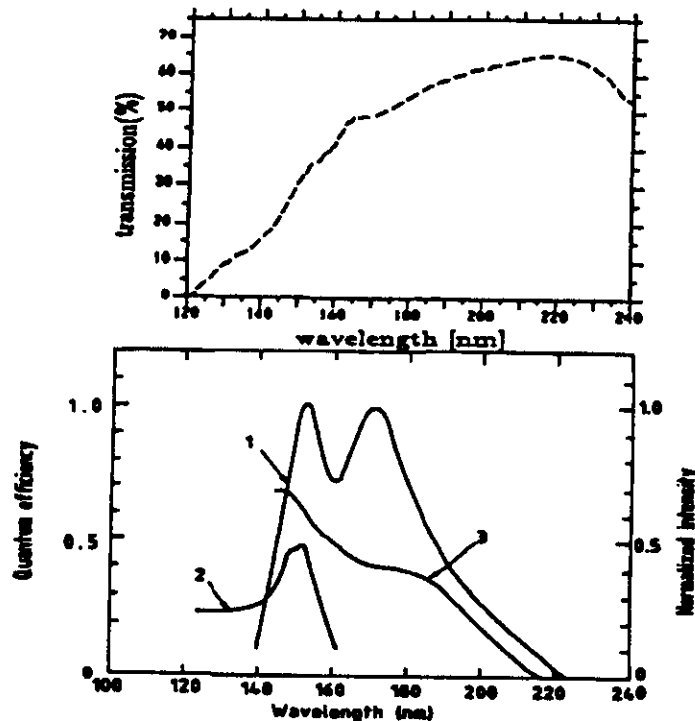


Figure I.7.6: Upper spectrum shows UV transmission of a 3.1 mm thick KMgF₃ sample not corrected for Fresnel reflections (adapted from ref. 10). In the lower emission the spectrum of KMgF₃ (1) and the quantum efficiencies of TEA (2) and TMAE (3) vapors are shown (adapted from refs. 209, 210).

nuclear physics or PET ²¹⁴ applications when count rates are very high and timing resolution is important. With its fast emission CsF was hoped to be a good substitute for BaF₂. It is however not only extremely hygroscopic (requiring hermetic packaging), but also, unfortunately, the few radiation damage tests performed gave only dismaying results, with a substantial damage seen already after a dose of 10 kRad ⁵⁵. It is however possible that this poor performance was totally due to impurities in the presently available samples and that this could be improved. In the high radiation dose applications CsF crystals would have to be encapsulated in containers with radiation-hard (quartz) windows.

BGO

BGO is the slowest of the various materials discussed here with its 300 ns decay constant. Until recently it was known to be sensitive to radiation, at least partly due to impurities which were present in the standard production-quality material. Bismuth germanate's main advantage is that it is a very dense scintillator (7.13 g/cm³). Because of this it is used in PET cameras ²¹⁵⁻²¹⁸ and in particle physics. There is much experience in the production of large quantities of BGO crystals. About 11,500 monocrystals have been grown for the L3 experiment at CERN ²¹⁹. Even before, in 1985 the 360-crystal CUSB-II BGO calorimeter at Cornell became operational, marking the first use of BGO in an electromagnetic calorimeter ^{220, 221}. For high rate/high dose applications, however, BGO

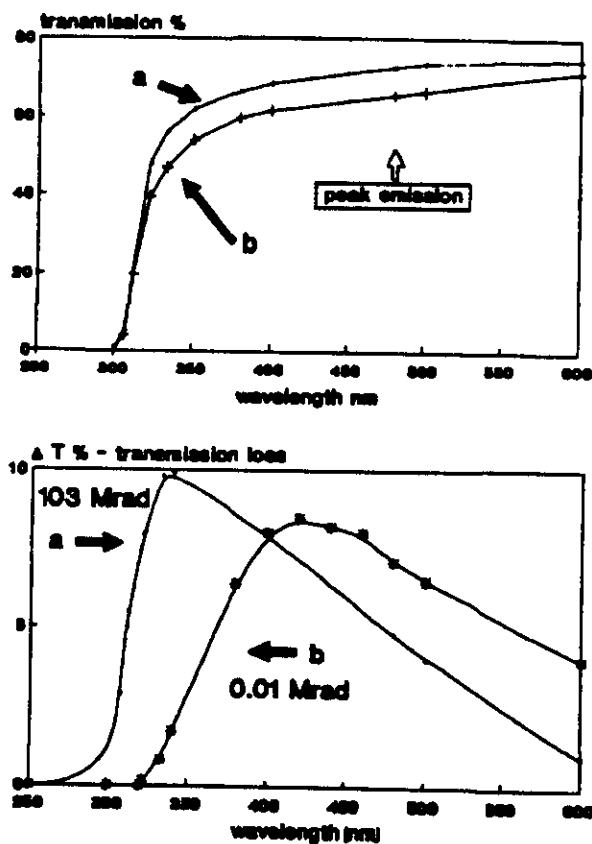


Figure I.7.7: Upper: the transmission curves of the 2.5 cm x 2.5 cm x 1 cm BGO crystal samples before (a) and after (b) gamma irradiation to a dose of 103 MRad; Lower: the comparison of transmission losses for the new samples (a) and the L3 1 cm x 1 cm x 2 cm thick samples 229.

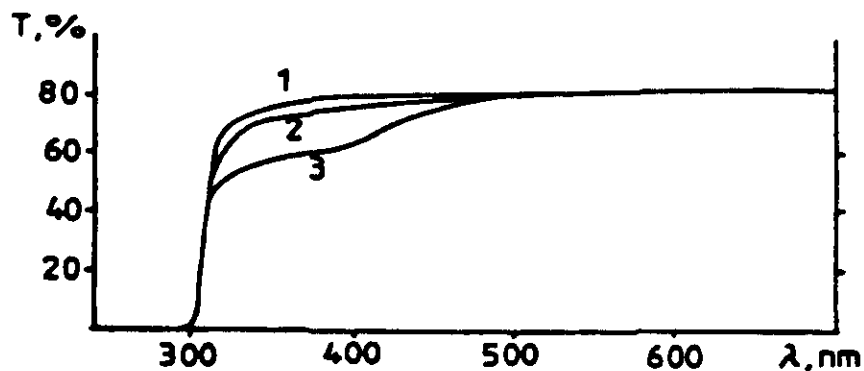


Figure I.7.8: Transmission spectra of the 5 mm thick BGO sample before (1) and after ⁶⁰Co gamma doses of 10⁷ Rad (2) and 10⁸ Rad (3) 146.

BGO samples was not final. Rather the technologically achieved level of radiation resistance in their work was due to limitations related to purity/price considerations. The BGO and other samples grown in that study had an impurity level of about 10⁻³.

In summary, it appears that the radiation resistance of BGO could be improved and highly radiation resistant large crystals may be available. The main drawback, however, is

color centers. Radiation damage due to color centers can be annealed not only by heating, but also by the use of violet-blue light sources ²³⁸.

It was suggested ^{6, 8, 239} that heavy fluoride glasses can have characteristics similar to the crystalline fluorides. They are excellent hosts for rare earth and cerium doping may result in scintillating glasses superior to oxide glasses. Some glasses contain BaF₂ as the major constituent and are expected to show the same type of fast luminescence transition. They have increased radiation resistance as compared to other glasses. Additionally, fluoride glasses are excellent media for fiber fabrication. Fluoride fibers have low transmission losses in the wavelength region above 2 μs Scintillator research can profit from the available body of data on fluoride glasses. A sublimation technique, for instance, was developed to reduce impurities such as iron and copper in the fluoride fiber material ²⁴⁰. This method may be applicable in the scintillating fluoride glass production.

The main anticipated difficulty is the selection of a proper host glass. The need is for a glass that would have a strong UV transparency to allow for transmission of short wavelength scintillation light. First cerium doped samples of heavy fluoride glasses were recently prepared in Europe, and a program of research is underway ⁸. These materials are potentially quite interesting because of cost considerations for large detectors.

I.8. Summary

In short summary BaF₂ and CeF₃ as scintillators and PbF₂ as a Cherenkov radiator seem to be at the present time the most promising radiation resistant and fast materials for high intensity applications. The lack of a slow component, a conveniently located emission spectrum, and a higher density make CeF₃ a more promising candidate, but production feasibility of large good quality crystals has still to be demonstrated. Also, for some applications even a 25 ns decay constant can be considered "slow". Possible mass production of large (25-50 cm) good quality crystals of barium fluoride is actively investigated and, provided that a solution will soon be found, this crystal scintillator seems to be the most serious available choice for high rate applications in the future large detectors.

One can expect that the present vigorous research on high density, fast and radiation hard crystal scintillators will continue. It is quite possible that many new and improved practical materials will appear quite soon, and it would not be surprising if some of the scintillators listed in Table I will prove to be better choices. In a recent review Van Eijk ¹¹ concluded that in the coming years the emphasis of scintillator research will be on the two groups of materials exhibiting either cross luminescence (fast scintillators) or materials with the 5d-4f transition luminescence (high light yield in the visible range). In general, developments in the technology of crystal production will lead to a marked improvement in the quality of crystals grown, dramatically reducing the level of impurities and defects. This in turn will permit the creation of efficient and fast crystal scintillators which will be able to survive the multi-MRad radiation doses to be encountered in the future high energy physics and nuclear physics experiments.

- Research Trends*, presented at the *International Symposium LUMDETR '91*, October 9-12, 1991, Riga, Latvia.
10. P. Dorenbos et al., *Photon Yields And Decay Times of Cross Luminescence in Ionic Crystals*, presented at the *1991 IEEE Nuclear Science Symposium*, Santa Fe, New Mexico, November 5-9, 1991.
 11. C. W. E. Van Eijk, *Fast Scintillators And Their Applications*, presented at the *International Symposium LUMDETR '91*, October 9-12, 1991, Riga, Latvia.
 12. S. E. Derenzo et al., *X-Ray Fluorescence Measurements of 412 Inorganic Compounds*, presented at the *1991 IEEE Nuclear Science Symposium*, Santa Fe, New Mexico, November 5-9, 1991.
 13. G. Finsel et al., *Nucl. Instr. and Meth.* **A290** (1990) 450.
 14. R. DeSalvo, *Hybrid Photomultiplier Tubes*, CERN LAA/HC/89-004.
 15. D. Winn et al., *Properties of Photodetectors for SSC Scintillating Calorimeters*, Proceedings of the *Symposium on Detector Research and Development for the Superconducting Super Collider*, 15-18 October, 1990, Fort Worth, Texas, World Scientific, 1991, p. 419.
 16. R. DeSalvo et al., *First Results on the Hybrid Photocathode Tube*, CERN-LAA-HC/91-, CERN-PPE/91-.
 17. A. M. Gorin et al., *Nucl. Instr. and Meth.* **A310** (1991) 251.
 18. L. K. van Geest and K. W. J. Stoop, *Nucl. Instr. and Meth.* **A310** (1991) 261.
 19. S. Nagamiya et al., *Construction of a Highly Segmented High-Resolution TOF System*, in Proc. *Fourth Workshop on Experiments and Detectors for a Relativistic Heavy Ion Collider*, Brookhaven, July 2-7 1990, BNL-52262, p. 433.
 20. J. P. Vivien, *Boules et Chateaux de Cristal: Detecteurs Multicompteurs $\gamma 4\pi$* , report CRN/PN83-25, Strasbourg, 1983;
F.A. Beck, in Proc. *Int. Conf. on Instrumentation for Heavy Ion Nuclear Research*, Oak Ridge, TN, USA, 22-25 Oct. 1984, ed. D. Shapira (Harwood Academic, 1985) p. 129.
 21. K. Wisshak et al., *Nucl. Instr. and Meth.* **A292** (1990) 595;
Nucl. Instr. and Meth. **A299** (1990) 60.
 22. R. Novotny, *IEEE Trans. Nucl. Sci.* **NS-38** (1991)379;
Neutral Meson Detection With the Photon Spectrometer TAPS, presented at the *1991 IEEE Nuclear Science Symposium*, Santa Fe, New Mexico, November 5-9, 1991.
 23. R-Y. Zhu, *Limits to the Precision of Electromagnetic Calorimeters*, invited talk at the *First International Conference on Calorimetry in High Energy Physics*, Fermilab, 29 October-1 November 1990, in Proceedings, p. 25, World Scientific 1991.
 24. H. B. Newman, *Precision Electromagnetic Calorimeters for The Superconducting Supercollider*, Proceedings of the *Symposium on Detector Research and Development for The Superconducting Super Collider*, Fort Worth, October 15-18, 1990, in Proceedings, p. 15, World Scientific, 1991.
 25. *A Precision BaF₂ Crystal Calorimeter for the Superconducting Super Collider, Research and Development Proposal and Progress Report*, The BaF₂ Collaboration, submitted to the SSC Laboratory, September 1991.
 26. P. Schotanus et al., *Nucl. Instr. and Meth.* **A238** (1985) 56'.
 27. M. Suffert and G. Charpak, *Influence of the Temperature on the Response of the Fast*

- the *First International Conference on Calorimetry in High Energy Physics*, Fermilab, 29 October-1 November 1990, World Scientific 1991, p. 286.
65. G. Tzanakos et al., *IEEE Trans. Nucl. Sci.* NS-37 (1990) 1599.
 66. D. F. Anderson et al., *Nucl. Instr. and Meth.* 217 (1983) 217;
Nucl. Instr. and Meth. 225(1984)8;
Nucl. Instr. and Meth. 228(1984)33.
 67. D. C. Imrie et al., *Nucl. Instr. and Meth.* A297 (1990) 179.
 68. J. Seguinot et al., *Nucl. Instr. and Meth.* A297 (1990) 133.
 69. D. C. Imrie et al., *Nucl. Instr. and Meth.* A310 (1991) 122.
 70. G. Charpak et al., *Nucl. Instr. and Meth.* A307 (1991) 63.
 71. V. Dangendorf et al., *Nucl. Instr. and Meth.* A308 (1991) 519.
 72. D. F. Anderson et al., *Technical Memo on New Results on CsI Photocathodes: Enhancement and Aging*, Fermilab TM-1753, September 1991.
 73. P. Fonte et al., *Nucl. Instr. and Meth.* A310 (1991) 140.
 74. V. Peskov and A. Zichichi, *A New Scintillator: LiBaF₃, Preliminary Tests*, presented at the *Workshop on New Technologies for Supercolliders*, Erice, Sicily, 15-20 September 1990, CERN-PPE/91-139, 3 June 1991.
 75. S. Kwan and D. F. Anderson, *Nucl. Instr. and Meth.* A309 (1991) 190.
 76. G. Charpak et al., *Study of BaF₂ Calorimeters in Future Hadron Colliders*, presented at the *8th Workshop of the INFN-ELOISATRON Project on Perspectives for New Detectors in Future Supercolliders*, Erice, 17-24 October 1989, CERN-EP/90-41, CERN/LAA/EC/90-005, 4 April 1990.
 77. E. Dafni, *Nucl. Instr. and Meth.* A254 (1987) 54.
 78. W. Klamra et al., *Nucl. Instr. and Meth.* A265 (1988) 485.
 79. V. Yanovsky and P. Kozma, *Nucl. Instr. and Meth.* A276 (1989) 659.
 80. P. Kozma and C. Hradecny, *Nucl. Instr. and Meth.* A254 (1987) 639.
 81. E. Lorenz et al., *Nucl. Instr. and Meth.* A249 (1986) 235.
 82. J. B. Czirr and E. Catalano, *Nucl. Instr. and Meth.* 143 (1977) 487.
 83. R. C. Taylor et al., *IEEE Trans. Nucl. Sci.* NS-33 (1986) 243.
 84. C. L. Woody et al., *IEEE Trans. Nucl. Sci.* NS-36 (1989) 536.
 85. P. A. Rodnyi et al., *Spectra and Models of Luminescence of Barium-Based Fluorides*, Internal Report IAE-4963/11, I. V. Kurchatov Institute of Atomic Energy, Moscow, 1989.
 86. R. Visser et al., *IEEE Trans. Nucl. Sci.* NS-38 (1991) 178.
 87. P. Dorenbos et al., *Nucl. Instr. and Meth.* A310 (1991) 236.
 88. P. Schotanus et al., *Nucl. Instr. and Meth.* A281 (1989) 162.
 89. P. Schotanus et al., *IEEE Trans. Nucl. Sci.* NS-36 (1989) 132.
 90. A. Lempicki et al., *Inorganic Scintillation Research*, Boston University, unpublished report, 1990.
 91. T. Shimizu et al., *IEEE Trans. Nucl. Sci.* NS-33 (1986) 370.
 92. S. Kubota et al., *IEEE Trans. Nucl. Sci.* NS-34 (1987) 438.
 93. S. Kubota et al., *Nucl. Instr. and Meth.* A270 (1988) 598.
 94. S. Kubota et al., *Nucl. Instr. and Meth.* A285 (1989) 436.
 95. D. F. Heath and Paul A. Sacher, *Appl. Opt.* 5 (1966) 937.
 96. M. Murashita et al., *Nucl. Instr. and Meth.* A243 (1986) 67.
 97. A. J. Caffrey et al., *IEEE Trans. Nucl. Sci.* NS-33 (1986) 230.

135. C. L. Melcher and J. S. Schweitzer, *IEEE Trans. Nucl. Sci.* NS-35 (1988) 876.
136. D. F. Anderson, *IEEE Trans. Nucl. Sci.* NS-36 (1989) 137.
137. D. F. Anderson, *Nucl. Instr. and Meth.* A287 (1990) 606.
138. L. E. Elias et al., *Phys Rev.* 8 (1973) 4989.
139. Yu. M. Aleksandrov et al., *Solid State Phys.* 29 (1987) 1896.
140. S. Kubota et al., *Mechanism of Luminescence from CeF₂ Excited by VUV Photons and Ionizing Charged Particles*, in *Radiation Detectors And Their Uses*, KEK Report 89-5, July 1989, p. 104.
141. W. W. Moses and S. E. Derenzo, *IEEE Trans. Nucl. Sci.* NS-36 (1989) 173.
142. W. W. Moses and S. E. Derenzo, *Nucl. Instr. and Meth.* A299 (1990) 51.
143. A. J. Wojtowicz et al., *Cerium Compounds as Scintillators*, contribution to the 1991 IEEE Nuclear Science Symposium, Santa Fe, New Mexico, November 5-9, 1991.
144. M. Kobayashi et al., *Cerium Fluoride, a Highly Radiation-Resistive Scintillator*, KEK Preprint 90-140, November 1990, submitted to *Nucl. Instr. and Meth.*
145. M. Kobayashi et al., *R&D on Compact, Fast and Radiation-Hard Materials for Total Absorption EM-Calorimeters*, Presented at the Workshop "Physics at UNK", Serpukhov, USSR, September 25-28, 1990, KEK Preprint 90-130.
146. G. I. Britvich et al., *Nucl. Instr. and Meth.* A308 (1991) 509.
147. H. Ishibashi, *Nucl. Instr. and Meth.* A294 (1990) 271.
148. T. Utsu and S. Akiyama, *J. of Crystal Growth* 109 (1991) 385.
149. M. Kobayashi et al., *Nucl. Instr. and Meth.* A306 (1991) 139.
150. M. Kobayashi et al., *Nucl. Instr. and Meth.* B61 (1991) 491.
151. H. Ishibashi et al., *IEEE Trans. Nucl. Sci.* NS-36 (1989) 170.
152. K. Takagi and T. Fukuzawa, *Appl. Phys. Lett.* 42 (1983) 43.
153. C. L. Melcher et al., *IEEE Trans. Nucl. Sci.* NS-38 (1991) 506.
154. C. L. Melcher et al., *IEEE Trans. Nucl. Sci.* NS-37 (1990) 161.
155. S. Kubota et al., *Nucl. Instr. and Meth.* A268 (1988) 275.
156. B. K. Utts and S. E. Spagno, *IEEE Trans. Nucl. Sci.* NS-37 (1990) 134.
157. C. L. Woody et al., *IEEE Trans. Nucl. Sci.* NS-37 (1990) 492.
158. P. Schotanus et al., *IEEE Trans. Nucl. Sci.* NS-37 (1990) 177.
159. S. Keszthelyi-Landori et al., *Nucl. Instr. and Meth.* A303 (1991) 374.
160. R. B. Murray and F. J. Keller, *Phys. Rev.* 137 (1965) A942.
161. J. B. Birks, *The Theory And Practice of Scintillation Counting*, (Pergamon, New York, 1964).
162. T. Towyama et al., *J. Phys. Soc. Japan.* 24 (1968) 1133.
163. E. Blucher et al., *Nucl. Instr. and Meth.* A249 (1986) 201.
164. E. Nordberg, *Performance of the CLEO II Csl Calorimeter*, presented at the Workshop on Physics and Detectors for KEK Assymmetric B-Factory, April 15-18, 1991.
165. *Proposal For a High Resolution Spectrometer For Neutral Mesons*, Los Alamos, December 1989.
166. W. G. Gong et al., *Nucl. Instr. and Meth.* A287 (1990) 639.
167. C. L. Woody et al., *Radiation Damage in Undoped Csl and Csl(Tl)*, presented at the 1991 IEEE Nuclear Science Symposium, Santa Fe, New Mexico, November 5-9, 1991.
168. J. A. Kierstead et al., *Progress Report on Generic R&D on Undoped Cesium Iodide*,

193. S. E. Derenzo et al., *IEEE Trans. Nucl. Sci.* NS-37 (1990) 203.
194. G. Charpak et al., *New Developments in Calorimetry Based on VUV Scintillators Coupled to Photosensitive Gaseous Detectors*, contribution to the *ECFA Study Week on Instrumentation for High-Luminosity Colliders*, Barcelona, 14-21 September 1989, CERN 89-10, ECFA 89-124, 593.
195. J. A. Valbis et al., *Opt. Spectrosc. (USSR)* 64 (1988) 1196 (in Russian); *Solid State Commun.* 67(1988)183.
196. V. Peskov and A. Zichichi, *A New Scintillator: LiBaF₃, Preliminary Results*, CERN-PPE/91-139, 3 June 1991.
197. P. Schotanus et al., *Detection of CdS(Te) Scintillation Light With Silicon Photodiodes*, presented at the *1991 IEEE Nuclear Science Symposium*, Santa Fe, New Mexico, November 5-9, 1991.
198. C. L. Melcher and J.S. Schweizer, *Cerium-Doped Lutetium Oxyorthosilicate: A Fast, Efficient New Scintillator*, presented at the *1991 IEEE Nuclear Science Symposium*, Santa Fe, New Mexico, November 5-9, 1991.
199. F. W. K. Firk, *Nucl. Instr. and Meth.* A297 (1990) 532.
200. W. W. Moses et al., *Scintillation Properties of Lead Sulfate*, presented at the *1991 IEEE Nuclear Science Symposium*, Santa Fe, New Mexico, November 5-9, 1991.
201. V. G. Baryshevsky et al., *Nucl. Instr. and Meth.* B58 (1991) 291.
202. S. I. Ziegler et al., *Characteristics of the New YAlO₃ Compared to BGO and GSO*, presented at the *1991 IEEE Nuclear Science Symposium*, Santa Fe, New Mexico, November 5-9, 1991.
203. P. Schotanus et al., *Nucl. Instr. and Meth.* A272 (1988) 913.
204. P. Schotanus et al., *Nucl. Instr. and Meth.* A284 (1989) 531.
205. P. Dorenbos et al., *IEEE Trans. Nucl. Sci.* NS-37 (1990) 119.
206. W. W. Moses and S.E. Derenzo, *Nucl. Instr. and Meth.* A299 (1990) 51.
207. W. W. Moses and S.E. Derenzo, *IEEE Trans. Nucl. Sci.* NS-37 (1990)96;
W. W. Moses et al., *IEEE Trans. Nucl. Sci.* NS-38 (1991) 648.
208. A. F. Buzulutskov et al., *Nucl. Instr. and Meth.* A288 (1990) 659.
209. G. Charpak et al., *New Scintillators for Photosensitive Gaseous Detectors*, presented at the *Symposium on Particle Identification at High-Luminosity Hadron Colliders*, 5-7 April, 1989, Fermi National Accelerator Laboratory, Batavia, USA, also CERN-EP/89-66.
210. G. Charpak et al., *BaF₂ Calorimeters With Photosensitive Gaseous Chambers*, contribution to the *ECFA Study Week on Instrumentation for High-Luminosity Colliders*, Barcelona, 14-21 September 1989, CERN 89-10, ECFA 89-124, Vol. 2, p. 588.
211. A. F. Buzulutskov et al., *Nucl. Instr. and Meth.* A281 (1989) 99.
212. A. F. Buzulutskov et al., *Nucl. Instr. and Meth.* A292 (1990) 546.
213. V. N. Makhov and N. M. Khaidukov, *Sov. Phys. Solid. State.* 32 (11) (1990) 1978.
214. N. A. Mullani et al., *IEEE Trans. Nucl. Sci.* NS-27 (1980) 572.
215. T. J. Spinks et al., *IEEE Trans. Nucl. Sci.* NS-35 (1988) 721.
216. H. Iida et al., *IEEE Trans. Nucl. Sci.* NS-36 (1989) 1006.
217. J. E. Litton et al., *IEEE Trans. Nucl. Sci.* NS-37 (1990) 743.
218. R. Lecomte et al., *IEEE Trans. Nucl. Sci.* NS-37 (1990) 805.
219. R. Sumner, *Nucl. Instr. and Meth.* A265 (1988) 252.

**FAST SCINTILLATORS
FOR HIGH RADIATION LEVELS**

Part II

Plastic and Liquid Organic Scintillators

Part II: Plastic and Liquid Organic Scintillators

II.1 Outline

We begin with a fairly detailed outline of the scintillation mechanism in organic (plastic and liquid) scintillators. An understanding of the fundamental phenomena will allow one to design an appropriate scintillator suitable for the high rate, high radiation areas of the hadron colliders. Questions concerning fast timing capability, light output, energy resolution, etc., are answered with modern scintillators. The principle problem remains that of sufficient radiation tolerance. Hence, most of the article will concentrate on the problem of a creating a radiation-resistant scintillator that also meets the other requirements. As will be seen, the achievement of radiation tolerance can result in the loss in one or more other capabilities. We begin the discussion of the radiation problem by reviewing what radiation levels will most likely exist at the colliders. From there the discussion will proceed to the effects of radiation upon scintillators with particular reference to the optical changes in the base material. This section will also include discussion of the key parameters affecting the level of damage detected. A section detailing the experimental results will follow which explores various attempts at improving the radiation tolerance of scintillators while minimizing any degradation to other useful characteristics. From there, we apply the present knowledge to planned detectors. A specific discussion of liquid scintillator research is followed by an outline of present research activities which are underway exploring some of the more detector-specific issues. A final concluding section closes the article.

II.2 The Scintillation Phenomenon

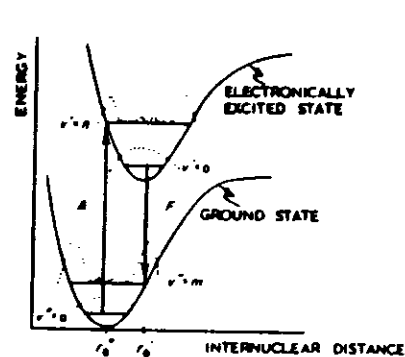
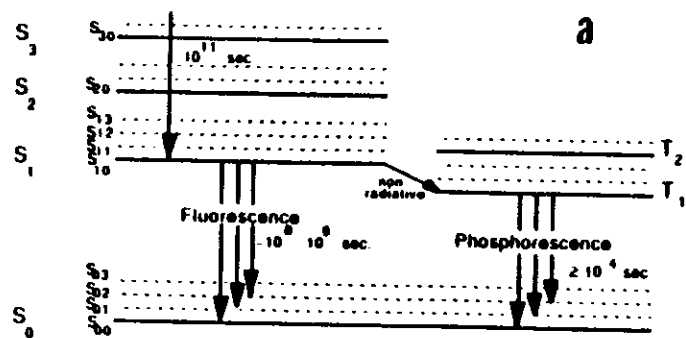
Scintillation is an exercise in applied photochemistry. It is useful to review the photochemical properties of the benzene molecule, as it forms the basis for all scintillation phenomena in organic plastics and liquids. Benzene contains six carbon and six hydrogen atoms. The carbon atoms have a ground state configuration of $1s^2 2s^2 2p^2$, but for binding, the configuration is $1s^2 2s 2p^3$, so that there are four valence electrons. Three of the valence electrons are hybridized into the trigonal (sp^2) configuration (figure 1). The electron wave functions are at angles of 120° to each other in a plane, giving the the benzene ring its planar hexagonal structure.

These three electrons form σ bonds, meaning that one has an electron pair (one from each adjoining carbon atom) shared in the area centered on a line joining the carbon atoms. The fourth valence electron (in a p -orbital) is a π electron, so that the bonding of the carbon atoms occurs by having the p -orbitals overlap in a

parallel fashion. A pair of electrons occupies the space both below and above the line joining the two carbon atoms. The double bonds of the benzene molecule are composed of one σ and one π bond. There are therefore only three double bonds within the benzene ring. It is known that each $C - C$ bond is equivalent, so the benzene molecule is considered to have a resonance hybrid structure whereby these three double bonds are shared equally among the six atoms. This is demonstrated in figure 2, along with the usual representation of a benzene ring drawn with a circle inside to reflect the π electron cloud resonance.

The π electrons form the basis for the scintillation mechanism. The π electron cloud is quantized into a series of singlet (S_{ij}) and triplet (T_{ij}) levels where $i = 0, 1, 2, \dots$ denotes the electron energy level and $j = 0, 1, 2, \dots$ denotes the vibrational sub-level. Figure 3 displays a representation of these energy levels. The fundamental luminescent properties arise from excitation of the molecule from the ground π states into the excited singlet and triplet states. Through non-radiative processes, there is de-excitation to the S_1 levels followed by a fast radiative transition to the ground S_0 states. This is known as *fluorescence*, and operates on a time scale of nanoseconds. It is also possible for an excited S_1 state to pass to an excited triplet T_1 state followed by a slow ($\approx 10^{-4}$ s) radiative decay to the ground state. Due to the difference in relative energy levels, this decay is at a longer wavelength than the fast fluorescent component. This phenomenon is known as *phosphorescence*. Finally it is also possible for a triplet T_1 state to pass to an excited singlet S_1 state followed by a fast radiative transition to the ground state. This is known as *delayed fluorescence* since it has the same spectral characteristics as the dominant fluorescent component. However since the transition probability for the triplet-singlet exchange is small, the time scale for the radiative transition is dominated by the initial spin flip process ($\approx 10^{-6}$ s). In liquid scintillators, it is probably the chief component of the tail in the scintillation decay time. It is also probably a major factor for plastic scintillators as well, but the fact of having a solid matrix complicates the extrication of all processes that contribute to the tail of the scintillation decay curve.

Given the presented information, one would deduce that the measured absorption would appear as in figure 4(a), when in fact they look more like figure 4(c). The sharp line spectrum of figure 4(a) corresponds to molecules at a very low pressure vapor phase. In a condensed phase, the fundamental energy levels can be split into many unresolved vibrational, rotational, and collisional substates (figures 4(b) and (c)). In addition, the absorption and emission spectra are split into different wavelength regimes by changes in interatomic spacing after excitation of the electronic



$$\text{STOKES LOSS} = (A - F)/2$$

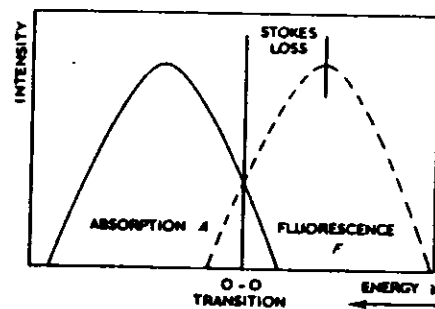
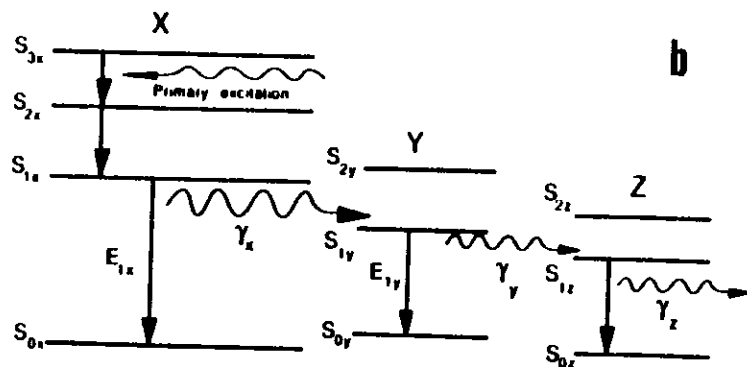


FIGURE 3: (a) The p electron energy levels. (b) An energy level representation of energy transfer in a scintillator composed of a solvent (X) plus two wavershifters (Y & Z). At higher concentrations (10^{-2} M), the dominant mode of energy transfer between X and Y becomes the non-radiative dipole-dipole interaction instead of the radiative mode shown in the figure. (c) Illustration of the how the Frank-Condon principle creates a shift between fluorescent absorption and emission. Note the definition of the Stokes shift. Figures 3(a) and (b) are adapted from reference [17]. Figure 3(c) is adapted from reference [19].

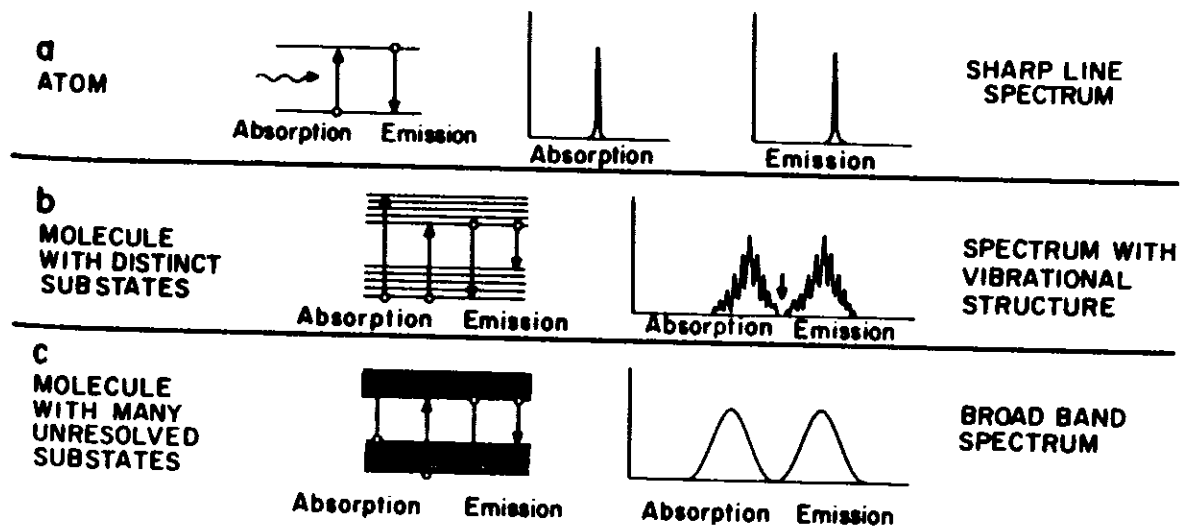


FIGURE 4: (a) Emission and absorption lineshapes for atoms at low pressure in a vapor phase. (b) The spectra for rigid molecules at low pressure in a vapor state. One can see how the formation of vibrational substates and the action of the internuclear potential (see figure 3(c)) creates Stokes shifted, broadened lineshapes. (c) Absorption and emission for typical molecules in a solvent with many unresolved substates. Adapted from reference [134].

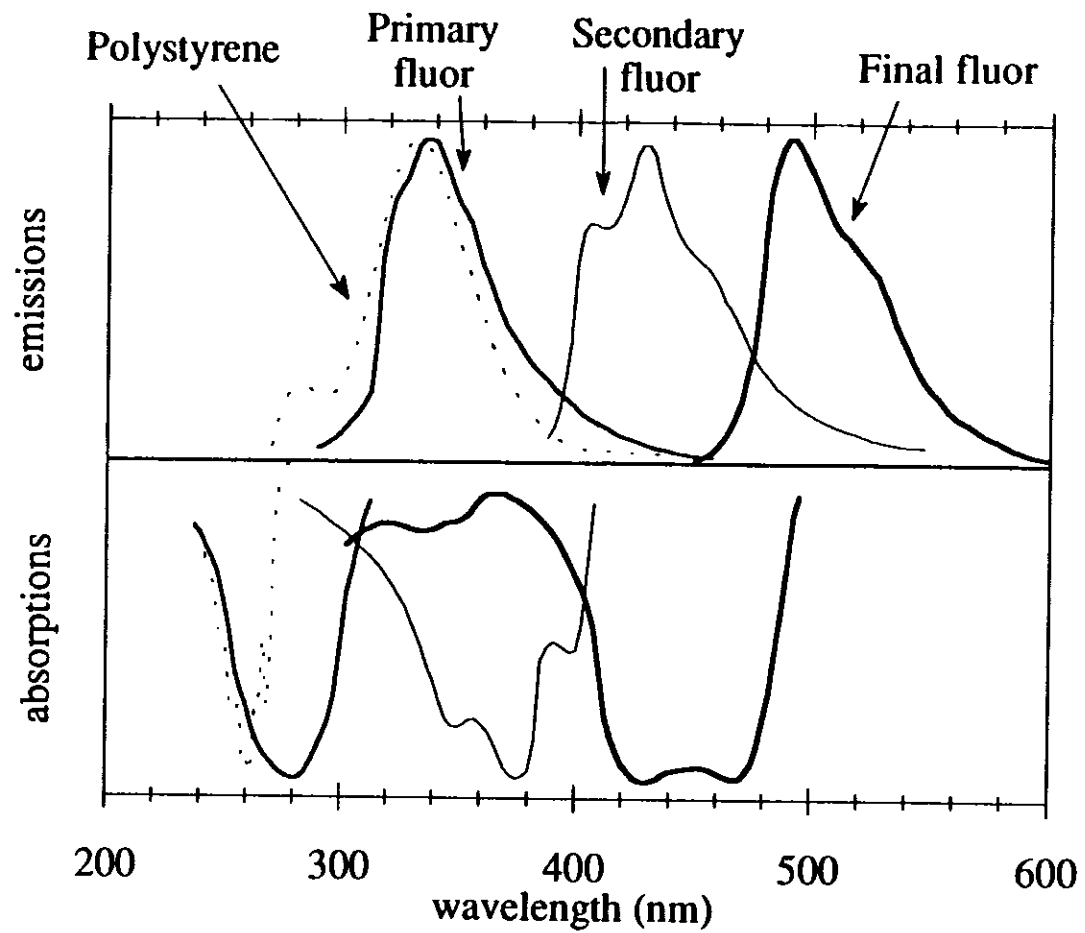


FIGURE 5: Illustration of how the matching of absorption and emission spectra create a green-emitting scintillator. Adapted from reference [135].

water and drying in air. The container is then immersed for several hours in a 30% solution of dichlorodimethylsilane/chloroform, and then rinsed in turn with chloroform, methanol, and distilled water followed by a final drying.

The doped styrene solution undergoes three freeze-thaw-pump cycles (using liquid nitrogen) to remove dissolved gases before having the polymerization process begun in a heated silicone bath. The heat bath has the following temperature profile: (i) 2 h @ 90°C, (ii) 24 h @ 110°C, (iii) 48 h @ 125°C, (iv) 12 h @ 140°C, (v) ramp down at 10°C/h to 90°C. At 125°C, the containers are backfilled with nitrogen gas to prevent boiling. The stage at 140°C is used to minimize the residual amount of monomer. After the heating cycle is completed, the samples are temperature quenched in liquid nitrogen to prevent the formation of vacuum bubbles (which occur if the cooling is allowed to take place slowly to room temperature), and to facilitate the easy removal of the finished scintillator. The finished forms can be machine cut and polished to the desired specification.

This is more or less the method used to make cast sheets as well as cylindrical preforms used in fiber production. In the former, polymerization takes place between flat sheets of glass in order to maintain good surface quality. Diamond mill sawing can be used to cut the sheets while maintaining high surface quality at the cut surface. For fibers, the finished cylindrical preform is placed snugly inside a tube of acrylic which will become the cladding for the fiber. A combination of heat and pressure is used to bond the surfaces together, and the heated preform is then drawn into the finished fiber. Fiber diameters can be as large as 3 or 4 mm but 0.5 to 1.0 mm is more typical. Special techniques can be used to produce extremely thin fibers of 30 μm diameter. (Essentially, the initial fibers are gathered together into a "fiber preform" and then redrawn into the much smaller diameter fiber.) Needless to say, there are many "tricks-of-the-trade" used in the production of a scintillating fiber. Although good fibers can be produced as of the time of this writing, many subtleties are under active investigation.

II.3 Radiation Damage to Organic Scintillators

II.3.1 Expected Radiation Levels

Traditionally, the question of radiation-induced damage to organic scintillators has been a moot point as the detectors only had to endure dosages well below the threshold of damage ($\approx 10^3$ Gy) observed in tests of small samples [2]. However, experiments utilizing very high particle fluxes [3] and the planned construction of the SSC and LHC hadron colliders have brought to the forefront the question of

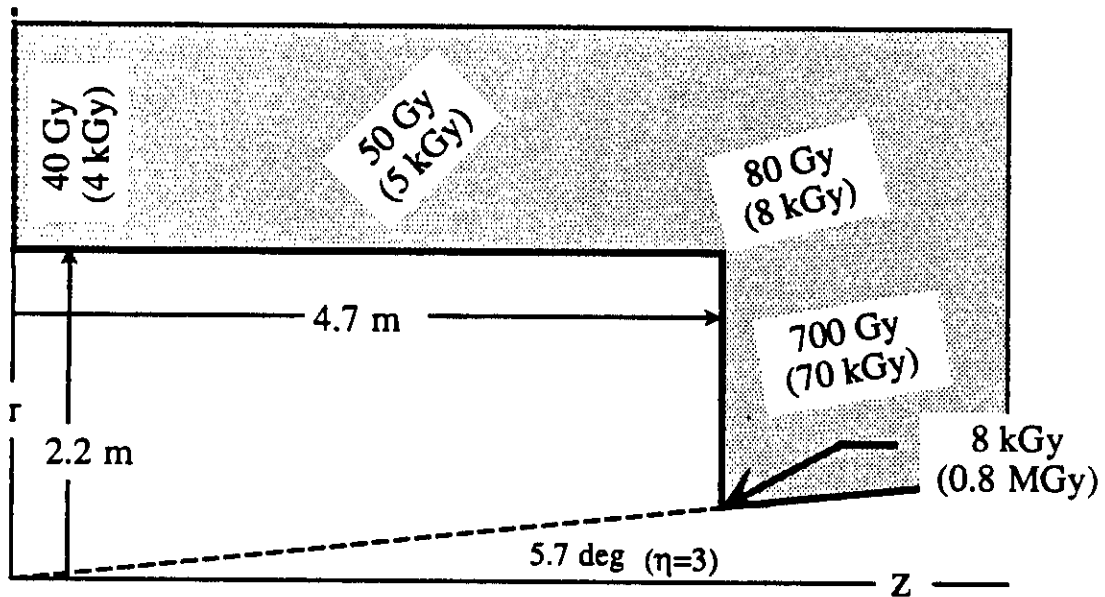
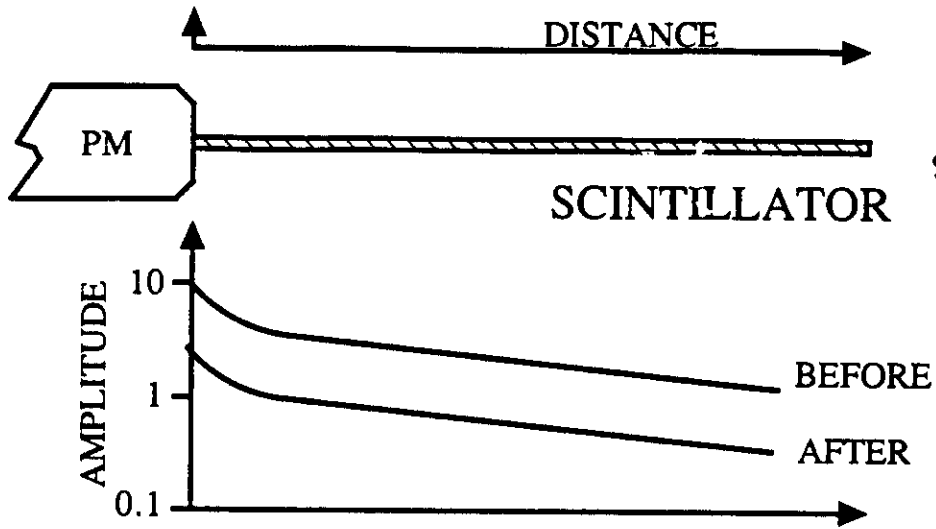
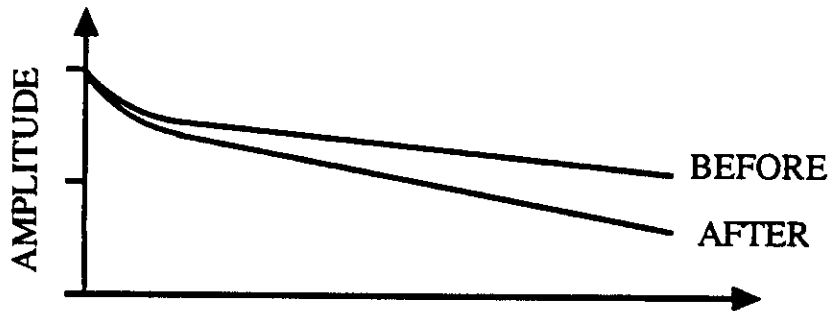


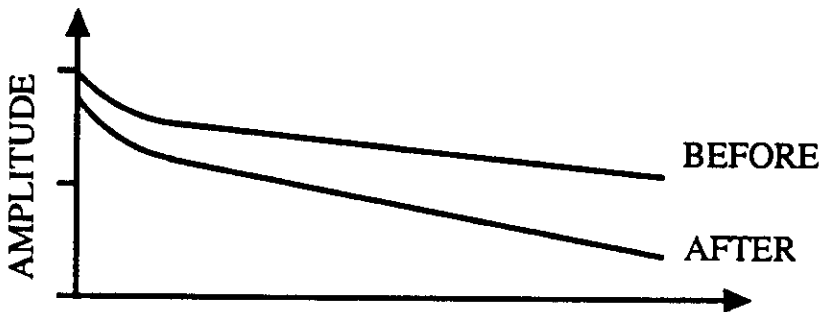
FIGURE 6: Estimates of the ionizing dose at electromagnetic shower maximum in the SDC detector at SSC design luminosity for one year, and in parentheses, at ten times the design luminosity for ten years. These doses are for the scintillator. Adapted from reference [11].



CASE 1: DAMAGE TO LOCAL SCINTILLATION YIELD ONLY



CASE 2: DAMAGE TO TRANSMISSION ONLY



CASE 3: TYPICAL DAMAGE OBSERVED IN EXPERIMENTAL CONDITIONS

FIGURE 7: Effect of radiation damage upon optical performance of scintillators. Adapted from ref. [8].

II.3.3 Damage Mechanisms

If one ignores any effect of irradiation upon the fluorescent molecules themselves, then one can examine the changes in light output solely as an effect due to the increased absorption induced in the base plastic. As figure 8 shows, the primary effect of radiation upon a sample of polystyrene is to add additional absorption centers in the UV and blue region, thereby creating an absorption "edge" which moves into the blue and yellow monotonically as a function of increasing dose (although strictly speaking, there is also some absorption in the green and red, but at a much smaller level). Since the mode of transfer between the base plastic and the primary fluor is non-radiative, this absorptive edge has no effect upon the initial energy transfer. However, as the edge moves into the longer UV, it interferes with the radiative transfer between the primary and secondary. (An alternate view of this is expressed in terms of the *transfer length* [24] needed to transfer $1 - e^{-1} \cong 63\%$ of the initial energy from the *donor* (the primary) to the *acceptor* (the secondary) molecule. For the typical concentrations used, the non-radiative mode has a transfer length ranging from 10-20 μm while the radiative mode is an order of magnitude larger.) Hence, barring any damage to the fluors and other additives, *the loss in light output can be solely explained in terms of absorptive changes in the base plastic leading to severe interference with the generation of the scintillation light.* In terms of the phenomena shown in figure 7, the strong increase in absorption in the UV leads to the drop in intrinsic light output while the much smaller but nonetheless significant increase of absorption in the blue and green results in the observed attenuation changes.

This idea was originally proposed from the results of experiments with the irradiation of liquid scintillators [25], and has been verified recently for typical plastic scintillators [14]. A qualitative verification of this model was seen in a study [26,63] in which the concentrations of the primary and secondary fluors were varied in order to ascertain the effect of fluor concentration upon the radiation resistance of the scintillators. Indeed, variations in the concentration of the primary fluor were found to have the most effect while the concentration of the secondary had no significant role. It is important to note that this does not mean that fluors cannot be damaged, nor that damaged fluors cannot contribute to formation of color centers. However, the commonly used ones do seem to bear up better than initially expected [27]. There are also cases of interesting new fluors that have turned out to be highly susceptible to irradiation, in particular when they are dissolved in a polystyrene base. These will be discussed later.

A critical result of this model is the proposed method of alleviating the problem. Ideally, one should use a highly soluble, highly efficient, radiation-resistant fluor whose absorption band spans the emission band of the plastic and whose emission is as red as possible (i.e., a large Stokes shift fluor), in effect creating what one researcher has termed an *intrinsic scintillator* [1,21]. At an appropriate concentration, the mode of transfer will be dominantly non-radiative, hence immune to the most severe optical changes occurring in the plastic. Finally the output will be shifted to sufficiently long wavelengths to avoid the secondary absorption effects. This ideal has to be modified by several observations: (1) as figure 9 shows, polystyrene has an absorption curve which falls until about 600 nm, hence the emission should preferably be in the range of 500 to 600 nm, (2) fast and efficient photodetectors with suitable quantum efficiency at those wavelengths are still only a research curiosity (although the research is very active!) [29-32], (3) longer wavelength fluors tend to get slower [19,22], and hence lose a critical feature for high energy physics applications (although the new "G" series of fluors from Bicorn seem to be a breakthrough in being fast (2-4 ns decay times), efficient, green-emitting (> 470 nm) waveshifters [33]).

The chemical mechanism for the damage to the polymer base is not completely understood although the general categories of reactions are known [1,20]. The most likely cause of the color centers is probably due to the presence of the *tertiary benzylic* hydrogen atom in polystyrene (and PVT) [34]. Figure 10 displays the reaction chain. This type of hydrogen atom, because of its placement in the molecule, is particularly susceptible to reactions with radicals formed from the irradiation of the polymer. This leads to the formation of polyenyl free radical chains whose absorption bands are a function of their length (for $n = 1$, $\lambda_{max}^{abs} = 260$ nm, while at $n = 5$, $\lambda_{max}^{abs} = 400$ nm). The recovery phenomenon seen after a high dose rate irradiation would be the slow (due to the large viscosity of polystyrene) recombination of these polyenyl radicals into short chains of polyenes within the main polymer backbone. The polyenes have their absorption bands at substantially shorter wavelengths (e.g., for $n = 1$: $\lambda_{max}^{abs} = 185$ nm, for $n = 5$: $\lambda_{max}^{abs} = 340$ nm). The polyenes would presumably be the source for the residual damage levels recorded after the initial annealing is completed. As likely as this model is (because it is based upon well-established chemistry), detailed and careful experimental studies will still be necessary to verify or refute it.

The most important parameters relating to radiation damage seem to be (a) dose, (b) dose rate, (c) atmosphere (i.e., presence of oxygen) before, during, and

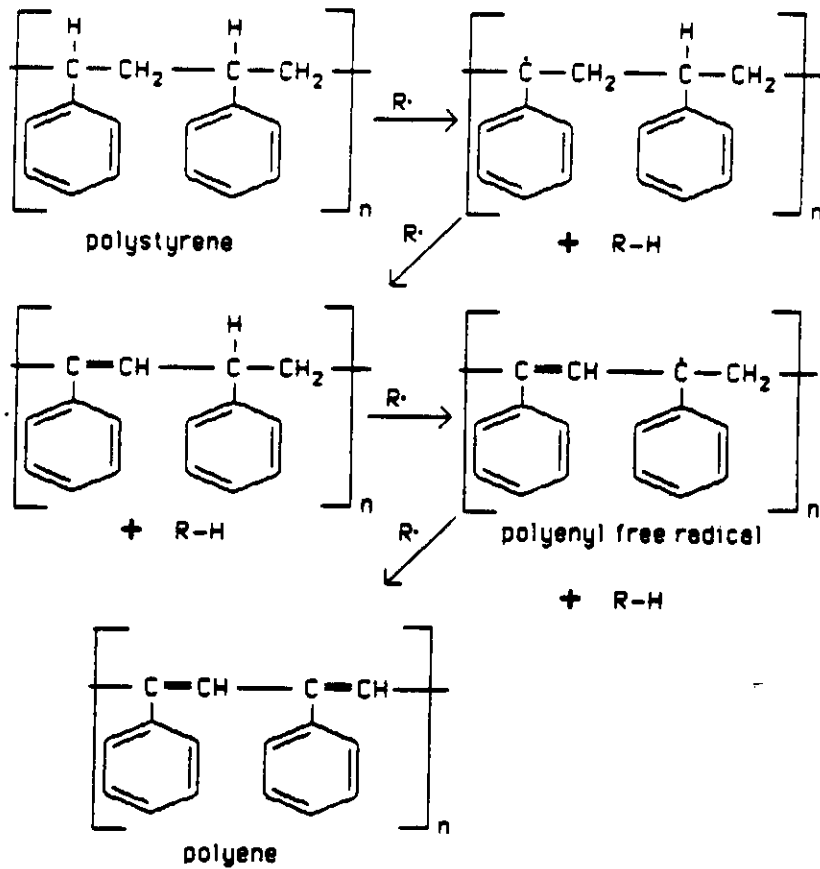


FIGURE 10: A likely candidate for the mechanism by which color centers are formed in polystyrene (and the related polyvinyltoluene). Adapted from reference [34].

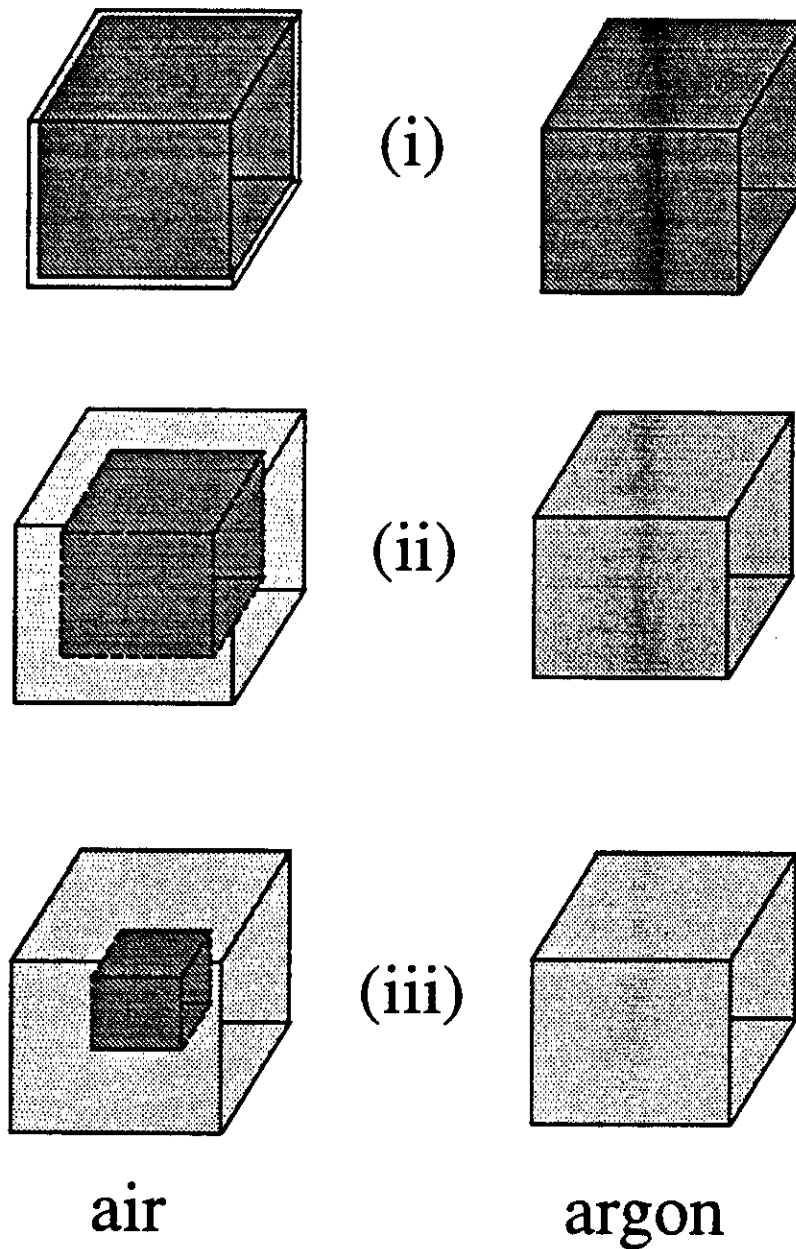


FIGURE 11: A pictorial representation of post-irradiation annealing in polystyrene cubes after a high dose rate irradiation. In air, oxygen diffusion drives the bleaching process at a rapid rate while in an oxygen-free atmosphere (e.g., argon), color center relaxation takes place slowly throughout the volume of the material. In air, the time scale from (i) to (iii) can be a matter of days while in argon the relevant time scale can be several months.

temperature (50 – 80°C) can increase this rate greatly [36,41] (figure 12). Unlike the foregoing case, the annealing takes place uniformly throughout the plastic. There is also a residual level of damage remaining after the completion of annealing. This residual level is larger as a function of the delivered dose.

The question that arises is whether this level of damage is the same as would occur if the same dose was delivered at a “realistic” rate (say over a period of at least a year). Very low dose rate experiments (< 10 Gy/hr) are now in progress and the full results are expected in the fall of 1991 and into 1992 [7,38,42]. As of this writing, some preliminary but nonetheless important results are available. These will be discussed later. First, we will review the indications given by previous studies.

One of the most relevant studies was performed by a sub-group of the ZEUS collaboration [40,43,44] upon polystyrene-based scintillators and acrylic-based wavelength shifters (WLS). In the case of the polystyrene-based scintillators, it was found that for a range of 30 Gy/hr to 10^4 Gy/hr, the level of damage was the same for a given dose (25 kGy) if complete annealing was allowed to take place (figure 13(a)). More importantly, online annealing was seen to take place (in air) since at the lower dose rates, less damage was observed immediately after irradiation than if the same dose was delivered at a much higher rate (figure 13(b)). In fact, the experimenters were able to find a dose rate (45 Gy/hr) for their thickness of scintillators (2.6 mm) for which they determined that the annealing formed an equilibrium with the permanent color center formation. On the other hand, they also reported [44] that for SCSN-38 [45] polystyrene-based scintillator, the loss in intrinsic light loss was twice as large for those samples irradiated in dry air as for those irradiated in an oxygen-free argon atmosphere. This seems to be indicative of a possible deleterious effect of oxygen during irradiation.

For acrylic, however, the effects are quantitatively different. A study [46] of acrylic-based scintillator used in a uranium/scintillator sampling calorimeter found that high rate tests underestimated the level of damage seen at a much smaller dose rate (in this case, due to the radioactive decay of the uranium absorber). In addition, this damage was greatly enhanced in the presence of oxygen. Figure 14 illustrates this result. The previously mentioned ZEUS group also noted that the annealing was much slower with the acrylic-based wavelength shifters. The high level of damage seen in these was attributed to the smaller diffusion coefficient for oxygen in acrylic (10 times lower than in polystyrene) and to the much higher levels of color center formation (a factor of 60) per unit dose compared to the polystyrene

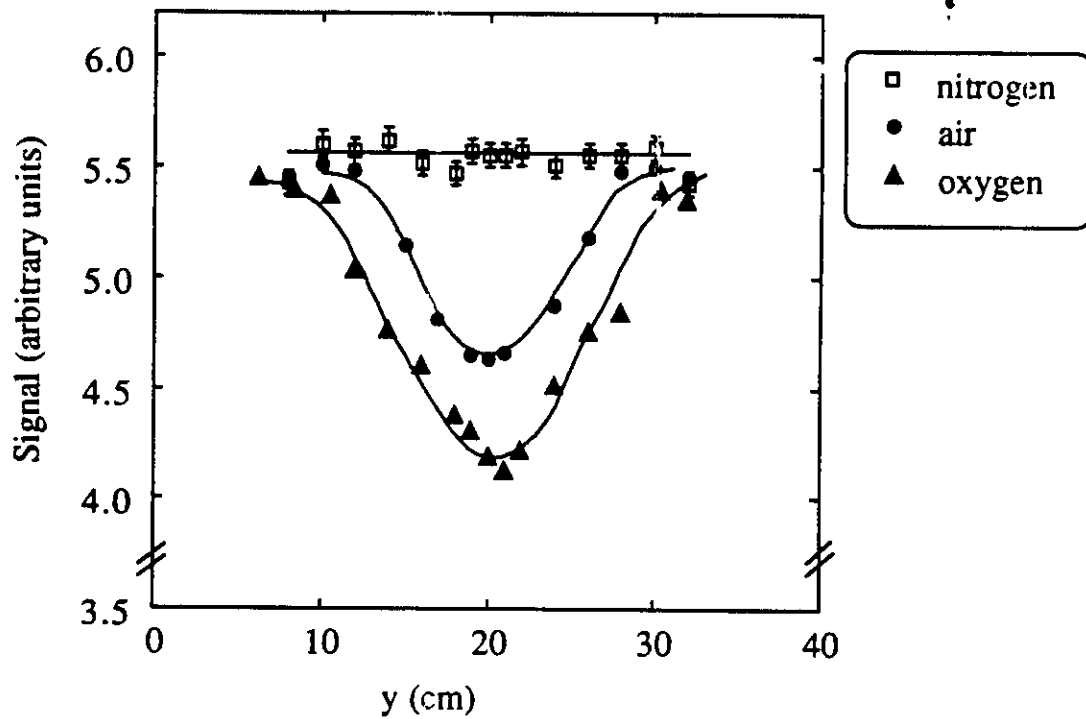


FIGURE 14: A demonstration of the destructive effect of oxygen during a low dose rate irradiation upon an acrylic based scintillator. A similar test at a high rate showed no such dependency upon atmosphere during irradiation. Adapted from reference [46].

Example of Fiber Irradiation (BCF-10 to 5 & 20 kGy)

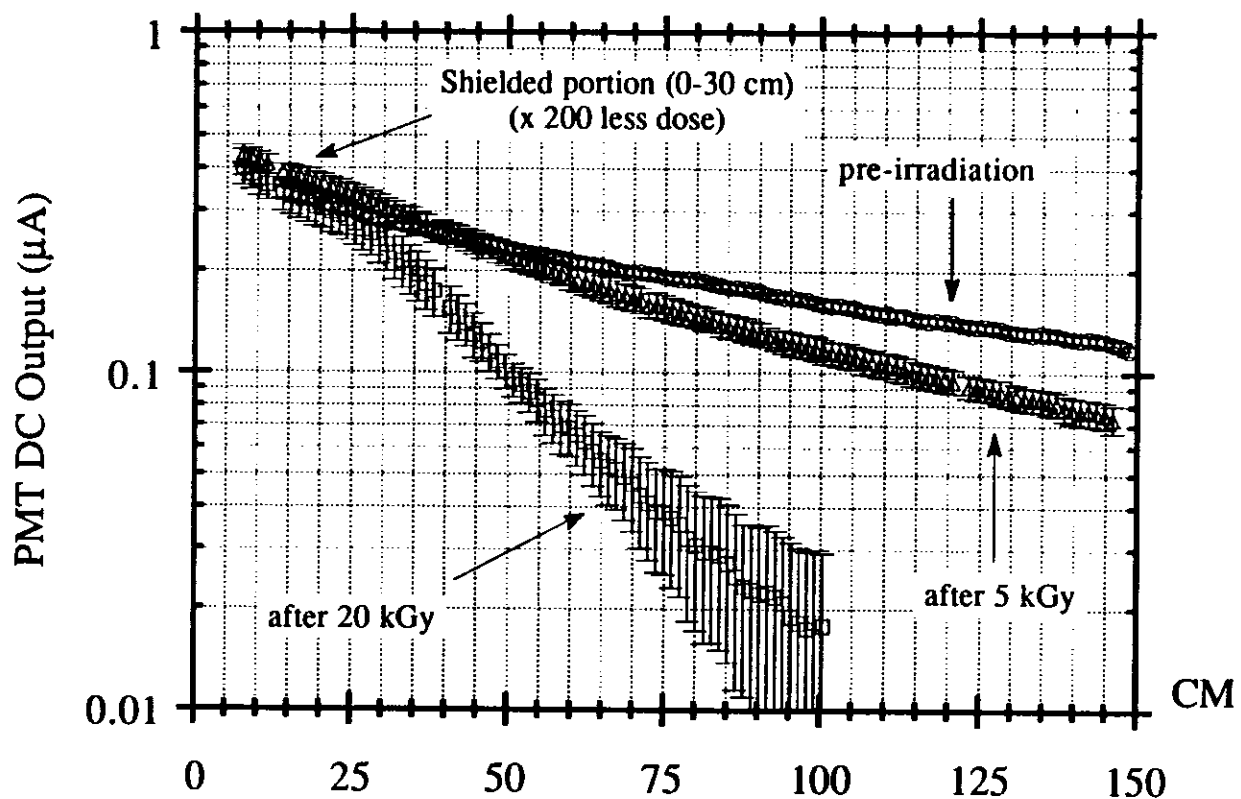


FIGURE 15: Typical data from a low dose rate (< 10 Gy/hr) irradiation of selected scintillating fibers.

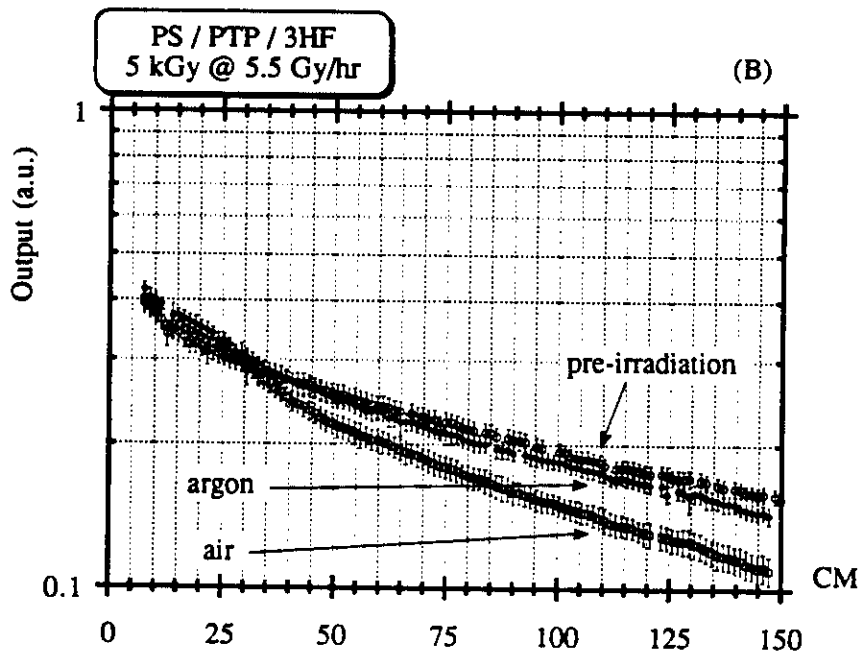
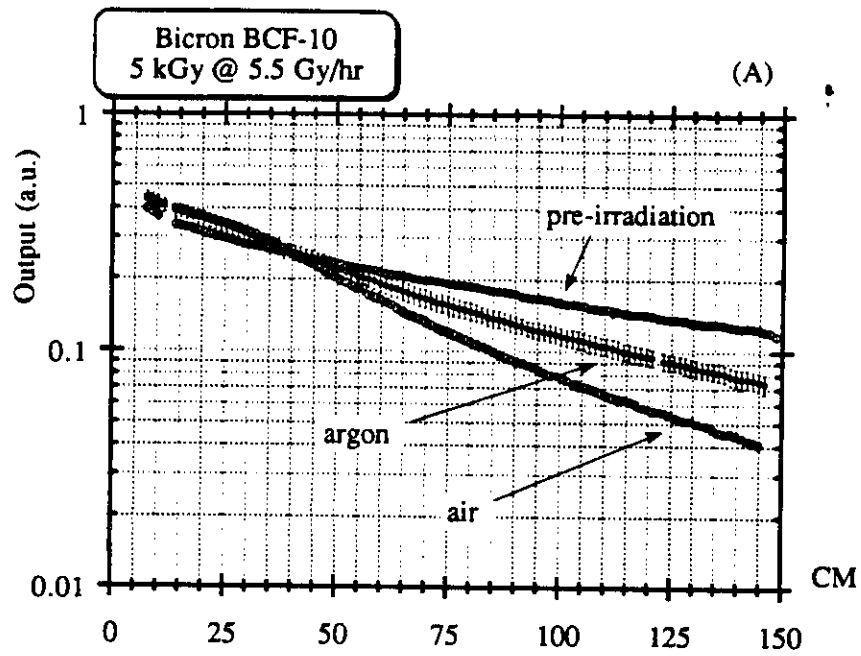


FIGURE 16: Some samples of data from a low dose rate irradiation of selected scintillating fibers (1 mm ϕ) in air and argon. The figures refer to (a) a blue and (b) a green-emitting fiber.

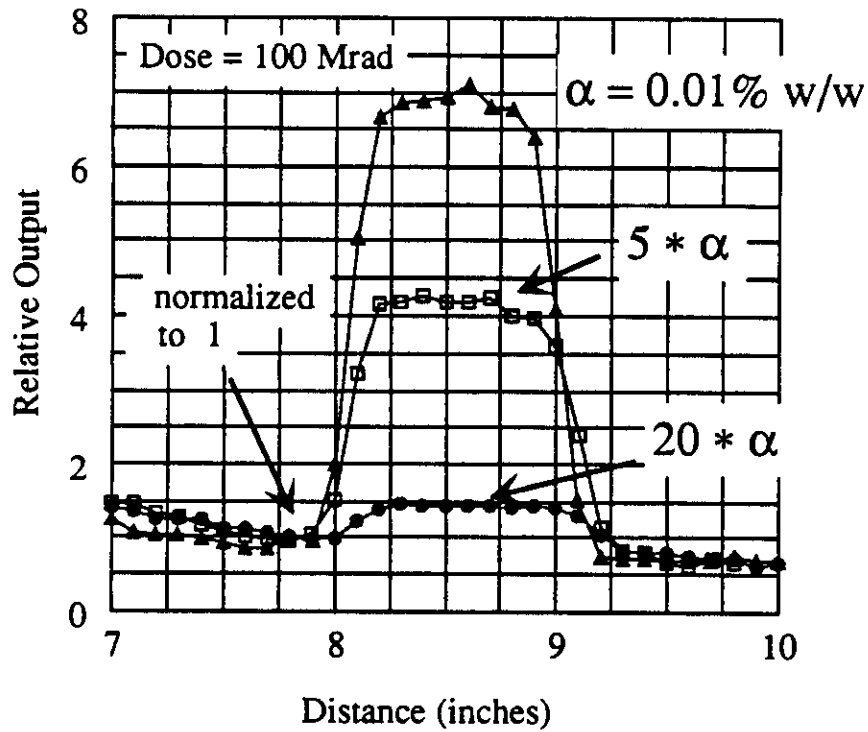


FIGURE 17: Effect of 3HF concentration upon intrinsic scintillation loss in a PS/PTP/3HF fiber. The larger the step size, the larger the loss in intrinsic light output. The use of increased concentrations of secondary fluors may minimize radiation damage in electromagnetic calorimeters. Adapted from reference [61].

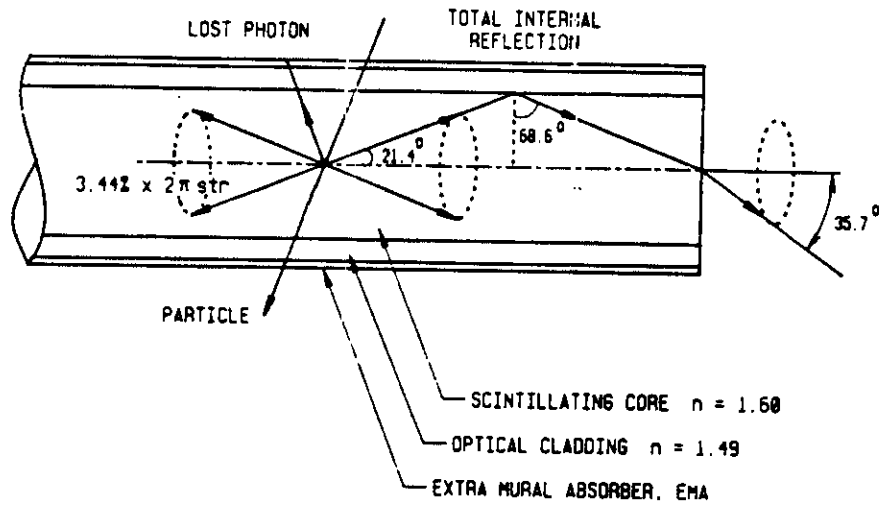
ting above 500 nm combining the positive aspects of PMP (solubility, low self-absorption, speed, quantum yield) and those of 3HF (emission above 500 nm, radiation resistance).

- (2) A two-step scintillator doped with two fluors, at least one of which must have a large Stokes shift: (i) a large Stokes shift primary emitting at 420-450 nm, and (ii) a secondary waveshifter with an emission preferably above 500 nm. This system may be useful for calorimeter systems that utilize active scintillator elements read out by waveshifter fibers. More about this will be said later.

II.3.6 Radiation Tolerant Bases

Another approach to improving radiation tolerance would be to find or synthesize a more radiation-tolerant plastic base. A study done some years ago [70] indicated that of the related materials polystyrene (PS), polyvinyltoluene (PVT), and polyvinylxylene (PVX), the order of radiation resistivity goes as $PVX > PVT > PS$. PVT is a well-known material for bulk scintillators, but it cannot be readily used in fiber form (which is of high interest at present). Although it may be the most radiation resistant, PVX seems to have some serious shortcomings, among them being the difficulty of polymerization and toxicity of the raw material. An initially hopeful candidate was polymethylphenylsiloxane [20,71-76]. This material has excellent optical qualities, one of them being radiation resistance. However, the solubilities of the standard fluors are extremely poor in it. This has resulted in the synthesis of a variety of oligophenylene fluors [20,34,68,71-73] which could be dissolved in sufficient quantities in this material. A result of this research is that some of these fluors may now form the basis of highly resistant *polystyrene*-based scintillators [67]. Efforts were also made to modify the structure of the siloxane material in order to improve its mechanical qualities as it tends to form elastomers [77,78]. Unfortunately, this seems to have resulted in serious degradation in the optical quality of the material. (Incomplete polymerization resulted in the formation of crystalline Rayleigh scattering centers giving the material inherently poor attenuation properties.)

Bicron has also produced an improved base material (RH-1) (not related to the aforementioned polysiloxane) which has undergone some promising preliminary tests of its radiation hardness when used as a base for blue-emitting scintillator [61,62]. It may be that a combination of this material (or a suitable improvement over it) doped with the new 'large Stokes shift fluors may produce the most radiation resistant plastic scintillator.



OPTICAL CLADDING THICKNESS: $>5\lambda$ (APPROX. 3 MICRONS)
 TYPICALLY 3-5% x O.D.

FIGURE 18: Schematic representation of a typical scintillating fiber. Adapted from reference [133].

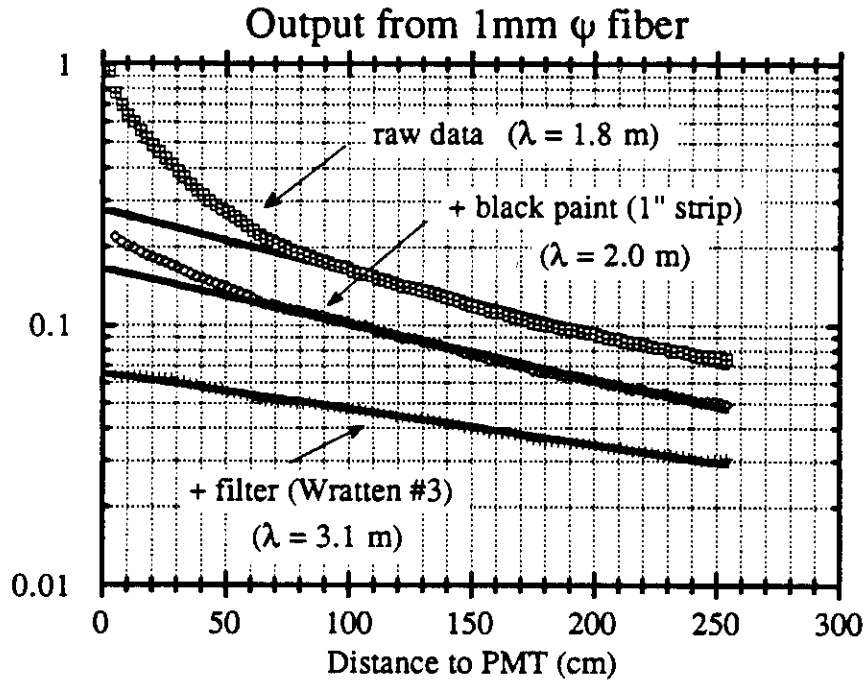


FIGURE 19: Typical attenuation behavior for a 1 mm fiber (SCSF-38). Cladding light creates a large but highly attenuated component near the readout end. Improved attenuation behavior can be achieved by absorbing this light with EMA and by optical filtering. In proposed tracking detectors, long lengths (several meters) of readout lightpipe fiber will have the same combined effect.

is no advantage to the alternate cladding. In addition, two atmospheres (air and argon) are being used to see (a) if oxygen is necessary for online annealing or will the color centers anneal on their own, and (b) can oxygen cause problems with the cladding and polystyrene core as noted above [41,47]. As noted previously, it seems clear that the presence of oxygen during irradiation at such a low dose rate leads to increased transmission damage over fibers irradiated in an essentially oxygen-free atmosphere.

For proposed tracking detectors utilizing scintillating fibers, both the amount of intrinsic scintillation output and attenuation length could be crucial to their performance since trackers will depend upon maximal detection of photons at the readout end of the detector. The large size of such a detector (several meters in length) will make the detection efficiency sensitive to any attenuation changes and loss in intrinsic light output. Fortunately, their position in the barrel region of the detector will allow them to escape the highest dose levels.

On the other hand, the electromagnetic calorimeters, particularly in the forward regions, will suffer the highest dose levels (> 10 kGy annually) due to the copious production of $\pi^0 \rightarrow \gamma\gamma$ decays which shower in the calorimeter. For electromagnetic showers, most of the deposited energy is concentrated within a relatively short longitudinal range within the calorimeter. Monte Carlo studies [64] have indicated that the loss in scintillation output will have the most effect upon the measured energy resolution. Attenuation changes will have little influence upon the measurement. In contrast, attenuation changes will be critical for hadronic calorimetry since the showers are spread over a much larger volume. In fact, maximal attenuation lengths are needed for such calorimeters to achieve their expected energy resolution. Hence changes in attenuation can drastically alter their performance. Another aspect comes from the fact that the source of the irradiation will likely have a different energy spectrum than the source of the interesting physics. Hence a true test of the performance should be based on testing the capability of the detector to "resolve" the physics of, say > 10 GeV particles after being irradiated with a 1 GeV beam [64].

Another proposed calorimeter uses small scintillation tiles read out by green waveshifter fibers [111]. The smallness of the tiles prevents the effects of attenuation from having too large an effect upon performance, while at the same time, the use of a green dye in the readout fiber minimizes attenuation. This system is currently undergoing development for the Solenoidal Detector Collaboration [10].

With regard to this approach, some recent results [67] on new scintillation

SCINTILLATOR ^a	λ^b (nm)	Light Yield				Ratio ^d
		Before	After	After 13 days ^c	After 53 days ^c	
MOPOM	420	0.90	0.05	0.48	0.56	0.62
MOPOM + 0.01% BBQ	470	1.08	0.15	0.72	0.81	0.75
MOPOM + 0.02% BBQ	470	1.09	0.18	0.78	0.86	0.79
MOPOM + 0.01% K27	500	1.08	0.31	0.85	0.94	0.87
MOPOM + 0.02% K27	500	1.08	0.31	0.85	0.96	0.88
O415A	415	1.05	0.56	0.90	1.00	0.96
O415A + 0.01% BBQ	470	1.15	0.48	0.98	1.10	0.96
O415A + 0.02% BBQ	470	1.16	0.39	1.01	1.13	0.97
O415A + 0.01% K27	500	1.10	0.65	0.99	1.09	0.99
O415A + 0.02% K27	500	1.13	0.60	1.00	1.11	0.99
O408	410	1.00	0.55	0.86	0.94	0.94
O408 + 0.02% BBQ	470	1.16	0.39	0.99	1.13	0.97
O408 + 0.02% K27	500	1.10	0.65	1.01	1.11	1.01
DAT	375	0.83	0.18	0.52	0.53	0.64
DAT + 0.01% DMPOPOP	430	0.98	0.35	0.80	0.85	0.87
DAT + 0.01% 3HF	530	0.97	0.46	0.72	0.78	0.81
PTP	360	0.96	0.24	0.47	0.48	0.50
PTP + 0.01% DMPOPOP ^e	430	1.00	0.58	0.81		

^a Fluor concentrations are by weight with the concentrations of the primaries at 1% (except for PTP and DAT which are at 1.25%).

^b Wavelength of peak emission.

^c First 10 days in oxygen and the remainder of the recovery time was in air.

^d The ratio is defined as *(After 53 days) / (Before)*.

^e Defined as the reference scintillator.

TABLE 1: The results of irradiating new fluor combinations doped in polystyrene to a total dose of 100 kGy. MOPOM is a fluor originally synthesized as a more radiation tolerant version of PMP. In a liquid base (1-phenyl-naphthalene), MOPOM was significantly more radiation resistant than PMP [56,122]. The oligophenylenes (O415A, O408, DAT) were originally synthesized as soluble fluors for polysiloxane-based scintillators [20,34,68,71-73]. Note in particular the exceptional performance of the sexiphenyls (O415A, O408). Such combinations may be worthy of study for tile/fiber calorimeters [111]. (The molecular formulae for the new fluors may be found in appendix II.A.) Adapted from reference [67].

length was reduced by 40%, and after 300 kGy, by over 60%. Comparing this with some data on 1 mm diameter plastic scintillating fibers [131], a blue-emitting fiber (RH-1) suffers a change of 75% in attenuation after 100 kGy, while a green-emitting fiber (SCSF-Y7) suffers a similar drop after only 30 kGy. A 3HF-doped fiber lost about 12% in attenuation after 30 kGy.

At the present time, the technique of using liquid scintillator seems highly promising and worthy of further development.

II.5 State of the Art

The most up-to-date information on the radiation resistance of scintillating fibers is found in data by the SPACAL [12,130], CEBAF [61,62], and FSU [131] groups. The latter two are continuing on from general studies of radiation damage in organic scintillators to more systematic tests of plastic scintillating fibers. Among these are (1) the effects of very low dose rates and the presence/absence of atmospheric oxygen (see figures 15 and 16), (2) the effect of different adhesives † ¶ (and a search for a suitable one that won't degrade the performance of the fiber), (3) defining a relationship between high and low dose rate tests, ‡ (4) testing new scintillator formulations, and (5) checking for variations within and between batches of a single formulation. The FSU group is also participating in studies of radiation-hard liquid scintillators [117] and in radiation tests for the SDC tile/fiber calorimeter project [10,111]. Both the CEBAF and FSU groups have also collaborated with the University of Illinois at Urbana-Champaign (UIUC) group (responsible for the JETSET electromagnetic calorimeter [105]) in performing some very preliminary radiation tolerance evaluations of a Pb/PSF (lead/plastic scintillating fiber) calorimeter [63]. This same UIUC group has performed some tests with the lead-eutectic design of

† A. Para, E. Skup, and G. Yasuda of Fermilab are carrying out an extensive survey of the effects of a wide selection of adhesives upon plastic scintillating fibers before and after irradiation.

¶ A group from Japan has recently published a report [137] on the transmission changes to various optical glues after doses of up to 10^6 Gy. Among the results, we note that the standard optical cement NE581 [138] shows no degradation above 400 nm after a 10^6 Gy exposure from an intense ^{60}Co source for a sample thickness of 10 μm .

‡ A group lead by N. Giokaris at Fermilab is also engaged in current tests comparing scintillators irradiated at high (12 kGy/hr) and low (1 Gy/hr) dose rates to identical doses.

[130]. The group plans further irradiation tests, particularly Pb/PSF calorimeter modules with electron beams of the appropriate energies.

II.6 Concluding Remarks

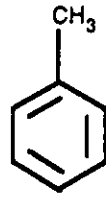
The present series of systematic investigations, if continued, should allow us to solidify our understanding of the effects of radiation upon scintillator performance to the point that for a given radiation environment (i.e., dose rate, atmosphere, temperature, etc.) and detector configuration, it may be possible to estimate (or even compute) the optimal combination of plastic base, fluors and fluor concentrations. Within the next few years we will probably have a variety of bases, with different strengths and weaknesses, and a palette of fluors to choose from. Most importantly we should have the quantitative understanding necessary to select the combinations most suitable to the physics goal.

ACKNOWLEDGEMENTS

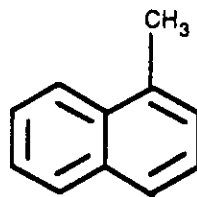
I would like to thank Dr. Kurtis Johnson of Florida State University for his critical appraisal and useful suggestions. I must also express my gratitude to Dr. Fabio Sauli of CERN for patiently awaiting the final version of this paper long after the original due date.

Liquid:

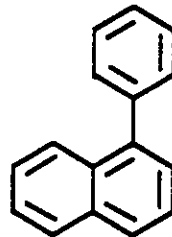
[5] Toluene



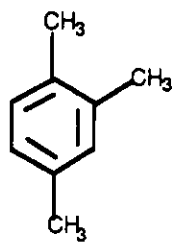
[6] 1MN 1-methyl-naphthalene



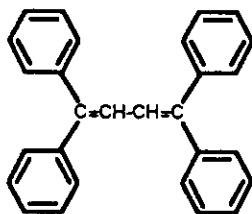
[7] 1PN 1-phenyl-naphthalene



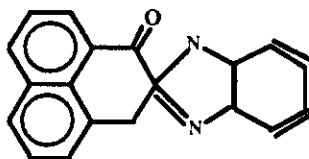
[8] pseudocumene



[3] TPB 1,1,4,4-tetraphenylbutadiene



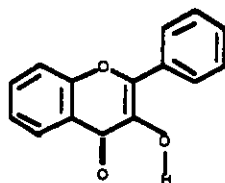
[4] BBQ 7H-benzimidazo[2,1-a]benz[de]isoquinoline-7-one



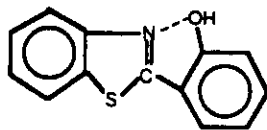
[5] Y7, K27 proprietary fluors

(D) Large Stoke Shift Fluors (>10,000 cm⁻¹)

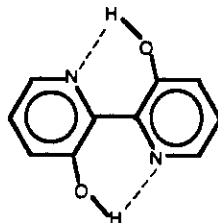
[1] 3HF 3-hydroxyflavone



[2] HBT 2-(2'-hydroxyphenyl)-benzothiazole



[3] BPD 2,2'-bipyridyl-3,3'-diol



References for Part II

- [1] A. Pla-Dalmau, "Design of Fluorescent Compounds for Scintillation Detection," doctoral thesis, Northern Illinois University (1990).
- [2] G. Marini et al., "Radiation Damage to Organic Scintillation Materials," CERN report 85-08 (1985).
- [3] P. Sonderegger, *Nucl. Instr. Meth.* **A257** (1987) 523.
- [4] D.E. Groom, "Radiation Levels in SSC Detectors," *Proceedings of the Summer Study on High Energy Physics in the 1990s*, ed. S. Jensen (World Scientific, Singapore, 1989) pp. 711-716.
- [5] A. Van Ginneken, "Estimated Radiation Levels in SSC Detectors," *Radiation Effects at the SSC*, ed. G.D. Gilchriese, SSC report SR-1035 (LBL, Berkeley, 1988) pp. 409-428.
- [6] H. Schönbacher, "Radiation Damage Studies for Detector Materials," *Proceedings of the ECFA Study Week on Instrumentation Technology for High Luminosity Hadron Colliders*, ed. E. Fernandez and G. Jarlskog, CERN report 89-10, pp. 129-151.
- [7] H. Schönbacher and F. Wulf, "Radiation Hardness Studies for the LHC Detector Materials," *Proceedings of the Large Hadron Collider Workshop*, ed. D. Rein and G. Jarlskog, CERN report 90-10 (Vol. I, 1990) pp. 289-324.
G.R. Stevenson, "New Dose Calculations for LHC Detectors," *ibid.*, (Vol. III) pp. 566-583.
- [8] S. Majewski, "Radiation Damage in Plastic Scintillators," *Proceedings of the Workshop on Calorimetry for the Supercollider*, ed. M.G.D. Gilchriese, (World Scientific, Singapore, 1990), pp. 451-485.
- [9] C. Zorn, *IEEE Trans. Nucl. Sc.* **37** (1990) 504.
- [10] Solenoidal Detector Collaboration, Expression of Interest to the SSC Laboratory (May 24, 1990).
- [11] D.E. Groom, "Ionizing Radiation Environment in SSC Detectors," *Proceedings of the Workshop on Radiation Hardness of Plastic Scintillator*, ed. K.F. Johnson (March 19-21, 1990, Tallahassee, Florida, U.S.A.) pp. 69-75.
- [12] A. Maio, "Effects of radiation damage on scintillating fibre calorimetry," *Proceedings of the Large Hadron Collider Workshop*, ed. G. Jarlskog and D. Rein, CERN report 90-10 (Vol. III, 1990) pp. 625-644.
- [13] W.L. Dunn et al., "Radiation Damage Studies of Straw Tube and Scintillating Fiber Elements," *Proceedings of the Symposium on Detector Research and De-*

- Scintillating Fiber Development for the SSC*, November 14-16, 1988, Fermilab, Batavia, Illinois, U.S.A., pp. 843-850.
- R. Ruchti, "Scintillating Fiber Detectors," *Proceedings of the Symposium on Detector Research and Development for the Superconducting Super Collider*, ed. T. Dombeck, V. Kelly, and G.P. Yost (World Scientific, Singapore, 1991) pp. 90-99.
- [30] B. Abbot et al., *IEEE Trans. Nucl. Sc.* **38** (1991) 441.
- [31] M. Salomon and J. Kitching, *IEEE Trans. Nucl. Sc.* **38** (1991) 140.
- [32] S. Reucroft et al., "Avalanche Photodiodes as Plastic Scintillating Fiber Read-out Devices," *Proceedings of the Symposium on Detector Research and Development for the Superconducting Super Collider*, ed. T. Dombeck, V. Kelly, and G.P. Yost (World Scientific, Singapore, 1991) pp. 287-289.
- [33] Bicron Corporation, Newbury, Ohio, U.S.A.
- [34] J.M. Kauffman, "Design of Radiation Hard Fluors," *Proceedings of the Workshop on Scintillating Fiber Development for the SSC*, November 14-16, 1988, Fermilab, Batavia, Illinois, U.S.A., pp. 677-740.
- [35] H. Schönbacher and W. Witzeling, *Nucl. Instr. Meth.* **165** (1979) 517.
- [36] C. Zorn et al., *Nucl. Instr. Meth.* **A276** (1989) 58.
- [37] C.S. Lindsey et al., *Nucl. Instr. Meth.* **A254** (1987) 212.
- [38] N.D. Giokaris, "Radiation Damage of the CDF Beam-Beam Counters during the 1988-89 Fermilab Collider Run," *Proceedings of the Workshop on Radiation Hardness of Plastic Scintillator*, ed. K.F. Johnson (March 19-21, 1990, Tallahassee, Florida, U.S.A.) pp. 121-125.
- M. Contreras and N.D. Giokaris, "Radiation Damage to SCSN23, SCSN81, and SCSN81+Y7 Scintillators," Fermilab CDF note 1341 (1991).
- N.D. Giokaris, "BBC Inefficiencies: Evidence from the Data and Bench Measurements," Fermilab CDF note 1214 (1990).
- [39] H. Hinrichs, *Z. Naturforsch.* **9a** (1954) 617.
- [40] K. Wick et al., *Nucl. Instr. Meth.* **A277** (1989) 251.
- [41] R.L. Clough and J.S. Wallace, "Radiation Effects on Organic Scintillators: Studies of Color Center Annealing," *Proceedings of the Symposium on Detector Research and Development for the Superconducting Super Collider*, ed. T. Dombeck, V. Kelly, and G.P. Yost (World Scientific, Singapore, 1991) pp. 661-665.
- [42] C. Zorn et al., "Results of a Preliminary Low Dose Rate Irradiation of Selected Plastic Scintillating Fibers," *ibid.* pp. 666-668.

- [65] J. Badier, "Electromagnetic Shower Resolution in a Scintillation Fiber Calorimeter," *Proceedings of the Workshop on Radiation Hardness of Plastic Scintillator*, ed. K.F. Johnson (March 19-21, 1990, Tallahassee, Florida, U.S.A.) pp. 77-84.
- [66] J. Badier, "Radiation Damage and Resolution Loss in Scintillating Fiber Calorimeters," *Proceedings of the Large Hadron Collider Workshop*, ed. G. Jarlskog and D. Rein, CERN report 90-10 (Vol. III, 1990) pp. 661-665.
- [67] A.D. Bross et al., "New Scintillation Materials for Fiber Tracking and Calorimetry," published in the Conference Record of the 1990 IEEE Nuclear Science Symposium (1990) pp. 132-136.
A.D. Bross et al., *Nucl. Instr. Meth.* **A307** (1991) 35.
- [68] J.M. Kauffman and M.A. Aziz, "Progress on Design of Radiation-Hard Scintillators," *Proceedings of the Workshop on Radiation Hardness of Plastic Scintillator*, ed. K.F. Johnson (March 19-21, 1990, Tallahassee, Florida, U.S.A.) pp. 29-48.
- [69] M. Kasha et al., "Molecular Electronic Criteria for Selection of Radiation-Hard Scintillators," *ibid.* pp. 49-60.
- [70] V.D. Bezuglii and L.L. Nagornaya, *J. Nucl. Eng.* **19** (1965) 490.
- [71] M. Bowen et al., *IEEE Trans. Nucl. Sc.* **36** (1989) 562.
- [72] M. Bowen et al., *Nucl. Instr. Meth.* **A276** (1989) 391.
- [73] M. Bowen et al., "Preliminary Results with a Polysiloxane-based, Radiation Resistant Plastic Scintillator," *Proceedings of the Workshop on Scintillating Fiber Development for the SSC*, November 14-16, 1988, Fermilab, Batavia, Illinois, U.S.A., pp. 785-797.
- [74] V.M. Feygelman et al., *Nucl. Instr. Meth.* **A290** (1990) 131.
- [75] V.M. Feygelman et al., *Nucl. Instr. Meth.* **A295** (1990) 94.
- [76] J. Harmon and J. Walker, "Siloxane Scintillators," *Proceedings of the Workshop on Radiation Hardness of Plastic Scintillator*, ed. K.F. Johnson (March 19-21, 1990, Tallahassee, Florida, U.S.A.) pp. 61-68.
- [77] J.P. Harmon and J.K. Walker, "A Review of Polymeric Scintillator Materials for Use at the SSC," *Proceedings of the Symposium on Detector Research and Development for the Superconducting Super Collider*, ed. T. Dombek, V. Kelly, and G.P. Yost (World Scientific, Singapore, 1991) pp. 680-682.
- [78] C.W. Park et al., "Fabrication of a Step-Index Scintillating Optical Fiber by a Coextrusion Process," *ibid.* pp. 284-286.
- [79] K.F. Johnson and H.L. Whitaker, *Nucl. Instr. Meth.* **A301** (1991) 372.

- [94] D. Acosta et al., *Nucl. Instr. Meth.* **A305** (1991) 55.
 D. Acosta et al., *Nucl. Instr. Meth.* **A308** (1991) 481.
 D. Acosta et al., *Nucl. Instr. Meth.* **A309** (1991) 143.
- [95] H. Blumenfeld et al., *Nucl. Instr. Meth.* **225** (1984) 518.
- [96] H. Blumenfeld et al., *Nucl. Instr. Meth.* **A235** (1985) 326.
- [97] H. Burmeister et al., *Nucl. Instr. Meth.* **225** (1984) 530.
- [98] A. Bross et al., *Nucl. Instr. Meth.* **A286** (1990) 69.
- [99] S.J. Alvsvåg et al., *Nucl. Instr. Meth.* **A290** (1990) 320.
- [100] A.J. Rusi et al., *Nucl. Instr. Meth.* **A290** (1990) 109.
- [101] C.M. Hawkes et al., *Nucl. Instr. Meth.* **A292** (1990) 329.
 M. Kuhlen et al., "Study of Scintillating Fibers for a High Resolution Time of Flight System at the SSC," *Proceedings of the International Industrial Symposium on the Supercollider*, ed. M. McAshan (Plenum Press, New York, 1989) pp. 611-622.
 R. Stroynowski, "Light Propagation and Timing with Scintillating Fibers," Caltech preprint CALT-68-1668, to be published in the proceedings of the 2nd International Conference on Advanced Technology and Particle Physics, June 11-15, 1990, Como, Italy.
 M. Kuhlen et al., *Nucl. Instr. Meth.* **A301** (1991) 223.
- [102] C. Angelini et al., *Nucl. Instr. Meth.* **A277** (1989) 132.
- [103] J.A. Crittenden, *Nucl. Instr. Meth.* **A277** (1989) 125.
- [104] K. Takikawa, "Red-Green-Blue Scintillating Fiber Calorimeter," *Proceedings of the International Workshop on Solenoidal Detectors for the SSC*, April 23-25, 1990, Tsukuba, Japan, pp. 370-374.
- [105] D.W. Hertzog et al., *Nucl. Instr. Meth.* **A294** (1990) 446.
- [106] L.R. Allemand et al., *Nucl. Instr. Meth.* **225** (1984) 522.
- [107] F. Takasaki et al., *Nucl. Instr. Meth.* **A262** (1987) 224.
- [108] R.E. Ansorge et al., *Nucl. Instr. Meth.* **A273** (1988) 826.
- [109] H. Blumenfeld et al., *Nucl. Instr. Meth.* **A278** (1989) 619.
- [110] H. Blumenfeld et al., *Nucl. Instr. Meth.* **A279** (1989) 281.
- [111] G.W. Foster and J. Freeman, "Scintillating Tile/Fiber Calorimetry Development at FNAL," *Proceedings of the International Workshop on Solenoidal Detectors for the SSC*, April 23-25, 1990, Tsukuba, Japan, pp. 376-380.
 R. McNeil et al., "Scintillating Plate Calorimeter Optical Design," *Proceedings of the Symposium on Detector Research and Development for the Superconducting Super Collider*, ed. T. Dombek, V. Kelly, and G.P. Yost (World

- J. Bähr et al., *Nucl. Instr. Meth.* **A306** (1991) 169.
- [122] C. Kennedy et al., *IEEE Trans. Nucl. Sc.* **37** (1990) 144.
- [123] N.S. Bamburov et al., *Nucl. Instr. Meth.* **A289** (1990) 265.
- [124] J.L. Pinfold et al., *Nucl. Instr. Meth.* **A286** (1990) 345.
- [125] Alltech Associates Inc., Deerfield, Illinois, U.S.A.
- [126] Pennwalt Corporation, Philadelphia, Pennsylvania, U.S.A.
- [127] R. Bionta et al, "Liquid Scintillator Calorimetry," research and development proposal submitted to the SSC Laboratory (1990).
- [128] C. Da Viá, CERN, private communication.
- [129] Schott 8250 produced by Schott Glaswerke, Mainz, Germany.
- [130] D. Acosta et al., "Effects of Radiation Damage on Scintillating Fibre Calorimetry," CERN preprint PPE/91-45, submitted to Nuclear Instruments and Methods (1991).
- [131] V. Hagopian et al., "Radiation Damage Tests of New Scintillating Fibers and Plates," *Proceedings of the Symposium on Detector Research and Development for the Superconducting Super Collider*, ed. T. Dombeck, V. Kelly, and G.P. Yost (World Scientific, Singapore, 1991) pp. 674-676.
- K.F. Johnson et al., "Radiation Damage Tests of a Scintillating Fiber Calorimeter," *ibid.* pp. 672-673.
- D.W. Hertzog et al., "Can a Pb/SCIFI Calorimeter Survive the SSC?" *Proceedings of the Workshop on Radiation Hardness of Plastic Scintillator*, ed. K.F. Johnson (March 19-21, 1990, Tallahassee, Florida, U.S.A.) pp. 93-103.
- [132] D.W. Hertzog et al., "High Resolution Pb/SCIFI Calorimetry: Performance and Radiation Damage Studies," *Proceedings of the First International Conference on Calorimetry in High Energy Physics* ed. D.F. Anderson et al., (World Scientific, Singapore, 1991) pp. 135-148.
- [133] C.R. Hurlbut, "Development of New Scintillator Materials for the SSC," *Proceedings of the International Industrial Symposium on the Supercollider*, ed. M. McAshan (Plenum Press, New York, 1989) pp. 187-202.
- [134] N.J. Turro, *Modern Molecular Photochemistry* (Benjamin/Cummings Publishing Co., Inc., Menlo Park, California, 1978).
- [135] T. Kamon et al., *Nucl. Instr. Meth.* **213** (1983) 261.
- [136] M. Adinolfi et al., "A High-Resolution Tracking Detector based on Capillaries filled with Liquid Scintillator," CERN preprint PPE/91-66, submitted to Nuclear Instruments and Methods.
- [137] M. Kobayashi et al., *Nucl. Instr. Meth.* **305** (1991) 401.